RESEARCH ARTICLE

Transcriptome Remodeling in *Trypanosoma cruzi* and Human Cells during Intracellular Infection

Yuan Li[1], Sheena Shah-Simpson[2], Kwame Okrah[3], A. Trey Belew[1], Jungmin Choi[1], Kacey L. Caradonna[2], Prasad Padmanabhan[2], David M. Ndegwa[2], M. Ramzi Temanni[1], Héctor Corrada Bravo[3], Najib M. El-Sayed[1,3]*, Barbara A. Burleigh[2]*

1 Department of Cell Biology and Molecular Genetics, University of Maryland, College Park, Maryland, United States of America, 2 Department of Immunology and Infectious Diseases, Harvard School of Public Health, Boston, Massachusetts, United States of America, 3 Center for Bioinformatics and Computational Biology, University of Maryland, College Park, Maryland, United States of America

* elsayed@umd.edu (NMES); bburleig@hsph.harvard.edu (BAB)

Abstract

Intracellular colonization and persistent infection by the kinetoplastid protozoan parasite, *Trypanosoma cruzi*, underlie the pathogenesis of human Chagas disease. To obtain global insights into the *T. cruzi* infective process, transcriptome dynamics were simultaneously captured in the parasite and host cells in an infection time course of human fibroblasts. Extensive remodeling of the *T. cruzi* transcriptome was observed during the early establishment of intracellular infection, coincident with a major developmental transition in the parasite. Contrasting this early response, few additional changes in steady state mRNA levels were detected once mature *T. cruzi* amastigotes were formed. Our findings suggest that transcriptome remodeling is required to establish a modified template to guide developmental transitions in the parasite, whereas homeostatic functions are regulated independently of transcriptomic changes, similar to that reported in related trypanosomatids. Despite complex mechanisms for regulation of phenotypic expression in *T. cruzi*, transcriptomic signatures derived from distinct developmental stages mirror known or projected characteristics of *T. cruzi* biology. Focusing on energy metabolism, we were able to validate predictions forecast in the mRNA expression profiles. We demonstrate measurable differences in the bioenergetic properties of the different mammalian-infective stages of *T. cruzi* and present additional findings that underscore the importance of mitochondrial electron transport in *T. cruzi* amastigote growth and survival. Consequences of *T. cruzi* colonization for the host include dynamic expression of immune response genes and cell cycle regulators with upregulation of host cholesterol and lipid synthesis pathways, which may serve to fuel intracellular *T. cruzi* growth. Thus, in addition to the biological inferences gained from gene ontology and functional enrichment analysis of differentially expressed genes in parasite and host, our comprehensive, high resolution transcriptomic dataset provides a substantially more detailed interpretation of *T. cruzi* infection biology and offers a basis for future drug and vaccine discovery efforts.

Author Summary

In-depth knowledge of the functional processes governing host colonization and transmission of pathogenic microorganisms is essential for the advancement of effective intervention strategies. This study focuses on *Trypanosoma cruzi*, the vector-borne protozoan parasite responsible for human Chagas disease and the leading cause of infectious myocarditis worldwide. To gain global insights into the biology of this parasite and its interaction with mammalian host cells, we have exploited a deep-sequencing approach to generate comprehensive, high-resolution transcriptomic maps for mammalian-infective stages of *T. cruzi* with the simultaneous interrogation of the human host cell transcriptome across an infection time course. We demonstrate that the establishment of intracellular *T. cruzi* infection in mammalian host cells is accompanied by extensive remodeling of the parasite and host cell transcriptomes. Despite the lack of transcriptional control mechanisms in trypanosomatids, our analyses identified functionally-enriched processes within sets of developmentally-regulated transcripts in *T. cruzi* that align with known or predicted biological features of the parasite. The novel insights into the biology of intracellular *T. cruzi* infection and the regulation of amastigote development gained in this study establish a unique foundation for functional network analyses that will be instrumental in providing functional links between parasite dependencies and host functional pathways that have the potential to be exploited for intervention.

Introduction

The kinetoplastid protozoan parasite *Trypanosoma cruzi* is the etiologic agent of human Chagas disease. This parasite has a complex life cycle that involves hematophagous triatomine insects as vectors for transmission and a broad range of mammalian hosts including extensive domestic animal and sylvatic reservoirs [1]. Epimastigote forms of the parasite proliferate in the midgut of the insect vector and give rise to non-dividing, mammalian-infective metacyclic trypomastigotes that are shed in the feces of blood-feeding triatomine bugs and initiate infection in the vertebrate host. *T. cruzi* trypomastigotes actively penetrate a wide range of nucleated cell types, become enveloped in an acidified lysosome-like compartment [2] where they receive signals to differentiate into amastigotes [3]. Differentiating parasites gradually escape the lysosomal vacuole [4] and proliferate as amastigotes in the host cell cytosol for 3–5 days (Fig 1A) before differentiating back into trypomastigotes (referred to as tissue or tissue culture trypomastigotes to distinguish these from metacyclic trypomastigotes), which are released into the extracellular space/medium upon host cell lysis. Motile trypomastigotes disseminate infection via the lymphatics and bloodstream to distal sites where they undergo further cycles of intracellular multiplication, egress and reinvasion. Thus, at several key points in its life cycle, *T. cruzi* undergoes developmental reprogramming to adapt to different hosts and variable niches within hosts, however the mechanisms governing these adaptive processes are not well defined.

Cellular differentiation is controlled at multiple levels including, for most eukaryotic cells, initiation of gene transcription (eg. [5, 6]). In trypanosomatids discriminatory mechanisms for the initiation of transcription at individual loci is largely absent. Most protein-coding genes lack promoters and are transcribed as long polycistronic units that are processed into individual mRNAs [7–10]. Consequently, trypanosomes rely on post-transcriptional processes such as mRNA stability, translational efficiency and post-translational modification to coordinate developmental transitions and other adaptive responses encountered throughout their complex life cycles [11–15]. Despite the recent emphasis on mRNA translation efficiency as a primary
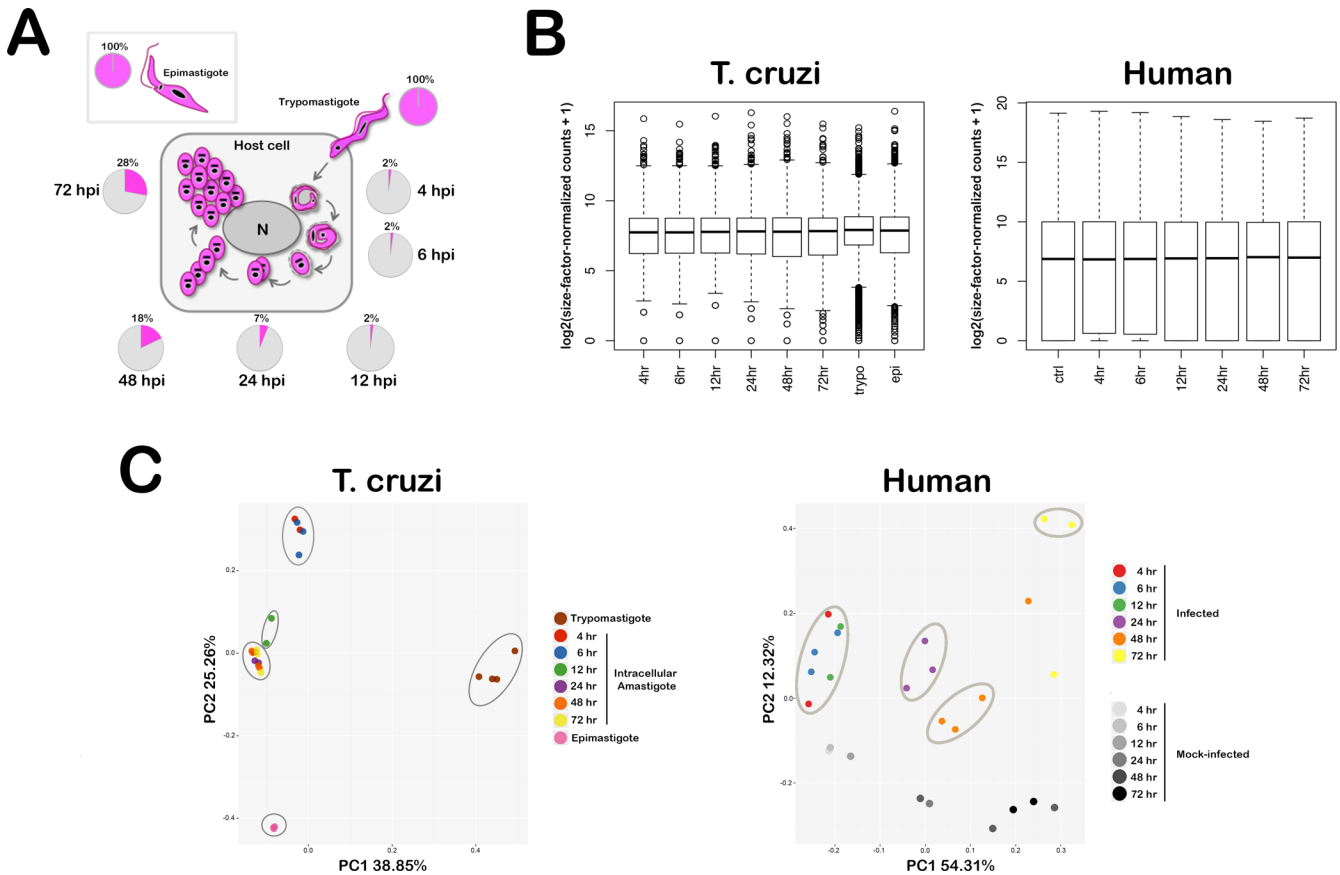
Fig 1. Simultaneous interrogation of parasite and host transcriptomes. (A) Intracellular *T. cruzi* life cycle and sample collection scheme.
Extracellular *T. cruzi* trypomastigotes actively penetrate mammalian cells where they receive cues to differentiate into amastigote forms that replicate in the host cell cytoplasm for 3–5 days, beginning at ~22 hpi with a doubling time of ~12 hr. Amastigote division ceases on day 4 or 5 post-infection and parasites differentiate back into trypomastigotes that rupture the host cell to initiate a new cellular infection cycle. For RNA-Seq analysis, total RNA was isolated from axenic *T. cruzi* epimastigotes (insect vector stage), extracellular trypomastigotes and from amastigote-containing human fibroblast monolayers at 6 time points spanning 4–72 hpi. Pie charts indicate the proportion of mapped sequence reads assigned to the parasite (pink) or human (grey). **(B) Distribution of global gene expression levels in a representative subset of *T. cruzi* and human samples.** Box plots showing comparisons of the distribution of per-gene counts (log2 counts per million with an offset of 1) normalized for sequencing library size. The ends of the whiskers represent the lowest datum still within 1.5 interquartile range (IQR) of the lower quartile, and the highest datum still within 1.5 IQR of the upper quartile. Genes with extremely high or low expression levels are shown as open circles above and below the whiskers, respectively. **(C) Principal component analysis plots of global transcriptome profiles.** Principal component analysis (PCA) plot for RNA-Seq data with *T. cruzi* and human samples plotted separately. The two first principal components (PC1 and PC2) are plotted with the proportion of variance explained by each component next to the axes labels. Each sample is represented by a dot and the color label corresponding to the sample group, such as the number of hours (hr) post-infection.

doi:10.1371/journal.ppat.1005511.g001

regulator of protein abundance in trypanosomatids [13, 16–18] and across eukaryotes more generally [19], there is strong evidence for the existence of post-transcriptionally generated mRNA regulons in *Trypanosoma brucei* and *Leishmania* that coordinate major developmental shifts in these organisms [20–23].

As with other eukaryotes, mRNA stability and translational efficiency are influenced by *trans*-acting factors (RNA-binding proteins: RBPs) that interact with *cis*-acting regulatory elements in the untranslated regions of trypanosomatid mRNAs (recently reviewed in [15, 24]). Because *trans*-acting factors regulate multiple mRNAs in a combinatorial fashion [25, 26], it has been challenging to identify *cis*-acting and *trans*-acting elements that are associated with the expression of functionally-regulated trypanosomatid genes [27]. However, a growing number of examples link candidate RBP expression levels with the modulation of mRNA subsets (eg. [15]). Indeed, an entire cellular differentiation program was shown to be triggered by the

over expression of a single RBP in African trypanosomes [28]. Functional *cis*-acting elements have been identified in a number of *T. cruzi* transcripts and associated with the regulation of expression in this organism [29, 30] including sets of developmentally-regulated [30–33] and functionally-related [34] genes. Although suggestive of the existence of mRNA regulons in *T. cruzi*, high-resolution transcriptomic data are needed to relate dynamic changes in parasite gene expression to functional adaptation on a global scale. Here, we exploit deep sequencing and informatics approaches to construct high-resolution transcriptome maps for three main *T. cruzi* lifecycle stages and include the simultaneous capture of parasite and host transcriptional responses during an intracellular infection of human fibroblasts by *T. cruzi*. With this approach, we gain deeper insights into the biology of *T. cruzi* with an emphasis on intracellular infection and conclude that transcriptome remodeling is required to alter the 'blueprint' upon which major developmental transitions are based.

Results/Discussion

Simultaneous capture of *T. cruzi* and human host cell transcriptomes by RNA-seq

To capture the global transcriptomic response associated with the establishment and maintenance of intracellular *T. cruzi* infection, RNA was isolated from low passage primary human foreskin fibroblasts (HFF) infected with tissue culture-derived *T. cruzi* Y strain trypomastigotes, and from mock-infected cells, at 4, 6, 12, 24, 48 and 72 hours post-infection (hpi) (Fig 1A). RNA was also generated from extracellular trypomastigotes and from axenically cultured log-phase *T. cruzi* epimastigotes for comparative purposes. Two to four independent biological replicates were sequenced for each condition generating 2.7 billion high quality reads from 35 samples (S1 Table) that were subsequently processed through our RNA-Seq and data analysis pipeline (S1 Fig). Sequence reads generated from *T. cruzi*-infected cell samples were resolved by mapping pre-processed reads against *T. cruzi* [35] and human hg19 reference genomes using the Tophat aligner program [36] (S2 and S3 Tables). The well-documented differences in transcriptional regulation between trypanosomes and humans [7, 8, 10] were reflected in the distributions of the log2-transformed and size-factor-normalized gene counts for both species (Fig 1B and S2 Fig). As expected, the fraction of total reads mapping to the *T. cruzi* genome from the mixed host-parasite read pool increased over time as intracellular amastigote replication ensued (Fig 1A). It is worth noting that due to the stringency imposed during mapping ($\leq$ 2 mismatches allowed/read) and the necessity to map *T. cruzi* Y strain sequences against a heterologous (CL Brener Esmeraldo) genome [35], the depth of coverage of the *T. cruzi* transcriptome at each stage (S1 Table) is most certainly underestimated. Despite this limitation, the demonstrated ability to resolve parasite and human sequences from a mixed read pool, and to obtain a high level of coverage of the *T. cruzi* transcriptome, bodes well for future transcriptomic analyses of the *T. cruzi* infection process *in vitro* and *in vivo*, particularly as whole genome sequence information for additional *T. cruzi* strains become available (eg. [37, 38]).

The overall reproducibility and experimental variation between similarly generated independent samples was evaluated with Pearson correlation (S3 Fig) and median pairwise correlation analyses for *T. cruzi* (S4 Fig) and human (S5 Fig) samples. For *T. cruzi*, biological replicates corresponding to each of the parasite developmental stages were highly correlated (S3A and S4 Fig), with the intracellular stages (from 4–72 hpi) exhibiting greater similarity to each other than to either of the extracellular stages (trypomastigotes and epimastigotes) (S3A Fig). The human transcriptome samples also displayed a high level of correlation between biological replicates (S3B and S5 Fig). One exception ("4hr2", HPGL0111), identified as an outlier

in a more systematic median pairwise correlation analysis (S6 Fig), was removed from down-stream analysis (S3B and S5 Figs).

To investigate general trends in the data while identifying and quantifying batch effects, principal component analysis (PCA) was carried out (Fig 1C) as well as hierarchical clustering of all parasite (S7A Fig) and human (S7B Fig) samples. PCA plots reveal a high degree of similarity between biological replicates for both the *T. cruzi* and human samples (Fig 1C). For *T. cruzi*, the extracellular parasite stages (trypomastigotes and epimastigotes) were well separated from each other and displayed very tight clustering within each group (Fig 1C; *T. cruzi*). The intracellular stages grouped according to their maturation status, with nascent amastigotes (4 and 6 hr) clustering together and well separated from the mature replicative amastigote stages (24, 48, 72 hr) with the 12 hr amastigotes in between (Fig 1C; *T. cruzi*). A similar trend is observed for the human data (Fig 1C; Human). Parasite-infected HFF samples are well separated from uninfected samples (PC2) and the early infection time points (4–12 hpi) clustered together (Fig 1C; Human). The later infection time points were more loosely clustered with outliers observed at 48 and 72 hpi (Fig 1C; Human). Notably, the transcriptome of uninfected fibroblasts changed considerably with time in culture (Fig 1C; Human PC1) underscoring the necessity to include mock-infected controls for each infection time course for direct comparison, as we have done here. Consistent with the PCA results, the unsupervised hierarchical clustering of *T. cruzi* samples (S7 Fig) labeled both by biological group and experimental batch date segregated trypomastigote, epimastigote and intracellular amastigote samples into distinct clusters. The partitioning of immature (4, 6, 12 hpi) and mature (24, 48 and 72 hpi) intracellular developmental stages of *T. cruzi* is also evident (S7A Fig). A similar partitioning of infected human cell samples into early (4, 6 and 12 hpi), mid (24 and 48 hpi) and late (72 hpi) time points suggest distinct phases of the host cell response to parasite infection (S7B Fig).

To extract biologically meaningful inferences from our expression data, lists of differentially expressed genes (DEGs) were constructed from pairwise comparisons of parasite or human expression data (S4 Table). As a large number of genes survived this initial cut-off (q-value < 0.05) a second filter (log$_2$fold-change $\geq$1.0) was imposed to identify gene expression changes with the highest potential impact (S4 Table) for *T. cruzi* developmental stages (S5 Table) and human fibroblasts at different stages of *T. cruzi* infection with matched controls (S7 Table). Because of frequent gene duplication and the presence of several expanded gene families in the *T. cruzi* genome, the parasite DEG data (S5 Table) was filtered to remove all but a single representative of each paralogous group (S6 Table). DEG information for *T. cruzi* (S6 Table) and human fibroblasts (S7 Table) were used for downstream Gene Ontology (GO) enrichment analysis [39, 40] and K-means clustering [41] (S1 Fig). Highlights from this collective analysis are presented and discussed in the context of the relevant biology of *T. cruzi*-host cell interactions in the following sections.

Transcriptomic signatures mirror biological features of *T. cruzi* developmental stages

Steady-state transcriptome data was generated for three distinct *T. cruzi* life stages with a more comprehensive analysis of intracellular amastigote development in human fibroblasts (Fig 1A). Focusing on the most disparate samples first, i.e. those derived from distinct developmental stages of *T. cruzi*: epimastigotes, trypomastigotes and intracellular amastigotes (24 hpi), we observed $\geq$2 fold differences in steady state transcript abundance for ~2000 to ~3500 parasite genes (S4 and S5 Tables) or between ~1500–2600 after correcting for paralogues (S4 Table). Thus, as a conservative estimate, we find stage-regulated changes in transcript abundance to occur for ~15–30% of the predicted protein-coding genes in the *T. cruzi* genome contrasting with a previous estimate of >50% derived from comparative microarray hybridization analysis of *T. cruzi* life stages [42].

Due to the nature of polycistronic transcription in *T. cruzi* [7–9] few parasite transcripts are expected to exhibit strict stage-specificity ie. detectable in one life stage and undetectable in others (Fig 1B). Despite this, we find a subset of *T. cruzi* genes (between ~135 and 350) to be over-represented at the transcript level in a single life cycle stage as compared to the other two developmental stages compared in this study (S8 Table). Adding weight to this approach, we observed the expected stage-selective expression of δ- and β-amastins in amastigotes and epimastigotes respectively (S8 Table). With the high proportion of hypothetical genes (>50% in each gene list; S8 Table) we were not able to identify significantly enriched GO terms associated with parasite stage-enriched genes. Nonetheless, some general observations offer insight into lifestyle differences among these different parasite stages. For example, trypomastigotes uniquely express a number of protein kinases and an intermediate filament-binding trichohyalin-like protein [43], which may reflect specialized capacities linked to host cell recognition, signaling and invasion by this parasite life stage [44–46]. Epimastigotes express twice as many genes in a stage-selective manner as the other parasite life stages (S8 Table), many of which encode metabolic enzymes (eg. pentose phosphate pathway, amino acid metabolism) or proteins involved in nutrient acquisition (eg. transporters of hexose sugars, nucleosides, folate/pteridine and amino acids). In contrast, amastigotes display elevated expression of cation transporters including (TcCLB.509197.39) which is upregulated early in amastigote development (by 6 hpi) with mRNA abundance reaching very high levels by 12 hpi (log$_2$fold-change 4.2; ~20-fold increase) to become the most highly expressed amastigote gene at 72 hpi (~35-fold increase) (S5 Table) as confirmed by qRT-PCR (S9 Fig). Another cation transporter gene (TcCLB.507527.50) that displays preferential expression in amastigotes at 24 hpi (S5 and S8 Tables) bears homology to the ferrous iron transporter characterized in *Leishmania amazonensis* [47], the expression of which is intimately coupled to amastigote development in this parasite. Thus, selective cation transporter expression, and potentially the need for iron uptake, may be a common feature of amastigote development and intracellular maintenance in both *Leishmania* and *T. cruzi*.

By virtue of their critical role in regulating gene expression in trypanosomatids [15], RNA-binding proteins (RBPs) represent another class of genes for which parasite stage-selective expression information is of interest. Only the RBPs that exhibit differential expression during the intracellular infection process are highlighted (S10A Fig). *T. cruzi* trypomastigotes selectively express two RBPs, RBP5 (TcCLB.511127.10) and RBP6 (TcCLB.506693.30) (S8 Table). While RBP5 has yet to be characterized, RBP6 has emerged as a critical regulator of metacyclogenesis in *T. brucei* [28]. Therefore, stage-specific expression of the orthologous gene in *T. cruzi* trypomastigotes suggests that TcRBP6 may exert important stage-specific functions in the non-dividing, cell-invasive forms of this parasite as well. While several RBPs exhibit transient and relatively low level increases in expression in developing amastigotes, a notable exception to this trend is TcCLB.504005.6 (S5 Table), for which mRNA abundance tracks with increasing intracellular amastigote numbers (S10 Fig). It is tempting to speculate that this particular RBP may participate in regulating processes critical to late stage amastigote growth or the next phase of the infection cycle that involves amastigote to trypomastigote conversion starting at ~96–120 hpi. Genome-scale dynamic mRNA expression data for RNA-binding proteins provides new and valuable information regarding the life cycle stage at which these important *trans*-acting mRNA regulatory factors are likely to act.

Extensive transcriptome remodeling in *T. cruzi* accompanies adaptation to life inside the mammalian host cell

To gain global insights into the intracellular *T. cruzi* infection process, a focused transcriptomic analysis was performed to capture dynamic changes in *T. cruzi* mRNA abundance as the

parasite established intracellular residence in mammalian host cells ([Fig 1A](#)). Extensive remodeling of the *T. cruzi* transcriptome was observed within the first 4 hours of trypomastigote invasion of human fibroblasts (2790 DEGs, [S4](#) and [S5](#) Tables), corresponding to the dramatic shift in environment and initiation of the amastigote differentiation program. More modest changes in *T. cruzi* transcript abundance occurred as amastigote development and maturation progressed over the next 20 hours of the infection cycle (644 DEGs in the 4–24 hpi interval) ([S4](#) and [S5](#) Tables). Then, once the amastigotes entered into replicative phase of the intracellular infection cycle (~22 hpi), few additional changes in the steady state transcriptome were detected (43 DEGs emerge in the 24–72 hpi interval; [S4](#) and [S5](#) Tables). While it is conceivable that a failure to detect additional DEGs at this stage is due to the masking of subtle transcriptome dynamics in asynchronously replicating amastigote populations, an alternative interpretation of this observation is that widespread transcriptome remodeling is only required to launch the *T. cruzi* amastigote differentiation program. Upon completion of the developmental switch, other important aspects of amastigote biology, such as nutrient acquisition and cell cycle regulation, are likely controlled by mechanisms other than mRNA stability. While we lack definitive data for this prediction, our observations align well with documented global gene expression patterns in related trypanosomatids, *T. brucei* [12, 48] and *Leishmania donovani* [11, 13, 23], where mRNA stability is cited as playing a more prominent role in early parasite development and both translation efficiency and post-translational modification acting as the main regulatory processes that control homeostatic functions [11, 13, 16–18, 23, 48].

Signatures of early *T. cruzi* amastigote development in mammalian cells

If transcriptome remodeling is required to generate a new blueprint to guide developmental transitions in *T. cruzi*, it follows that associated changes in morphology and functionality should be reflected in corresponding transcriptomic signatures. The capture of dynamic changes in parasite mRNA abundance over a time course of infection in human fibroblasts provides an opportunity to derive biological inferences based on differential expression patterns and to compare these with known aspects of *T. cruzi* amastigote biology. Focusing first on the early phase of intracellular infection by *T. cruzi* where the greatest number of DEGs was detected, we observe several expected features of the trypomastigote to amastigote transition in the transcriptome changes. These include: (1) rapid downregulation of transcripts encoding major polymorphic surface protein classes (trans-sialidases, mucins, MASPs and gp63) ([S4](#) and [S5](#) Tables Trypo vs Ama4), some of which have been implicated in host recognition, signaling and immune evasion [45, 49–51]; (2) reduced expression of genes involved in flagellar assembly and motility (within 4 hpi) ([S5](#) and [S9](#) Tables) coincident with dramatic shortening of the single *T. cruzi* flagellum; and (3) increased abundance of transcripts encoding the amastigote-specific surface protein, δ-amastin ([S5 Table](#)) [31, 52]. Consistent with the plasma membrane remodeling that is expected during trypomastigote to amastigote differentiation, we also observe significantly increased transcript levels for GPI-inositol deacylase (TcCLB.510289.40) [53], membrane-bound/secreted phospholipase A1 [54] (TcCLB.509011.90; [S5 Table](#)) and a surface-localized phosphatidylinositoI-phospholipase C (PI-PLC) (TcCLB.504149.160) [55] ([S5 Table](#)). Although central to parasite plasma membrane remodeling during differentiation [56], amastigote surface lipases are also well positioned to facilitate breakdown of the parasitophorous vacuole alongside the activity of a secreted hemolysin [57], analogous to the mechanism of vacuole egress by the intracellular bacterial pathogen, *Listeria monocytogenes* [58]. Moreover, once *T. cruzi* amastigotes become cytosolically-localized in mammalian cells there are ample opportunities for parasite surface and secreted/released products to interact with host molecules and to modulate host functions during the course of infection. In this regard, *T.*

cruzi amastigote phospholipase A1 can be considered a parasite-derived effector protein given that its expression is associated with perturbations in host cell phospholipid metabolism [59] and the activation of host protein kinase C [60].

In addition to remodeling at the plasma membrane during the early trypomastigote to amastigote transition, indicators of signaling pathway retooling also emerge in the transcriptome data (S5 Table; Trypo vs Ama4). For example, a number of predicted protein kinases and phosphatases are differentially expressed in the parasite shortly after trypomastigote entry into mammalian host cells (S5 Table; Trypo vs Ama4) including the previously characterized farnesylated protein tyrosine phosphatases (TcCLB.506743.130; TcCLB.506743.110) [61]. Consistent with the recognized role of cyclic AMP in *T. cruzi* differentiation processes [62], we also observe developmental regulation of central components of the cAMP-dependent signaling pathway, such as receptor-type adenylate cyclases (eg. TcCLB.511043.60; TcCLB.428999.20; TcCLB.507467.10), cAMP-dependent protein kinase A (TcCLB.509805.10; TcCLB.506227.150) and cAMP-dependent phosphodiesterases (eg. TcCLB.508277.100; TcCLB.506625.80) (S5 Table; Trypo vs Ama4). In the broader context of sensory detection and signal transduction, it is worth noting that 'ciliary and flagellar motility' emerges as an enriched GO term associated with mature *T. cruzi* amastigotes ($\geq$48 hpi) when compared to immature amastigote stages (S9 Table; eg. Ama4 vs Ama48). This signature is driven by the increase in mRNA abundance for several flagellum-associated protein coding genes in mature amastigotes after their initial decline during the initial stages of amastigote development (S10B Fig). The expression of the calcium-sensing FCaBP family members [63] in intracellular *T. cruzi* amastigotes suggests that the minimal amastigote flagellum may engage in sensory functions in the intracellular life stages, as suggested for *Leishmania* amastigotes [64]. As little is known regarding the mechanism(s) by which *T. cruzi* parasites detect and integrate sensory information, particularly for the intracellular mammalian-infective stages, the availability of high-resolution mRNA expression data for *T. cruzi* intracellular stages (S5 and S8 Tables) opens the door to discovery of additional parasite molecules that function in a sensory or signaling capacity including the many predicted protein kinases and phosphatases encoded in the *T. cruzi* genome [65] that have yet to be characterized.

Consistent with a period of rapid remodeling during early amastigote development in which proteins and membranes are expected to undergo extensive turnover, Gene Ontology enrichment analysis identified ribosomal RNA processing (GO:0006364), protein translation (GO:0006412) and protein folding (GO:0006457) as significantly enriched GO terms associated with nascent and developing amastigotes (S9 Table; Trypo vs Ama4-Ama12). Despite the fact that nascent intracellular amastigotes will not undergo a first round of replication for another ~20 hours, preparation for the eventuality of cell doubling is already evident in the transcriptome of early amastigote stages. Consistent with the projected increase in nucleic acid synthesis, nucleoside transporters (TcCLB.506203.10; TcCLB.506773.50) and enzymes involved in pyrimidine synthesis (eg. orotidine-5-phosphate decarboxylase; TcCLB.508373.29) and purine salvage are upregulated in immature amastigotes (S5 Table). Genes encoding enzymes in the guanine branch of the purine salvage pathway [66] are selectively upregulated in intracellular amastigotes as compared to trypomastigotes (eg. guanine deaminase: TcCLB.504431.100; inosine 5' monophosphate dehydrogenase (IMPDH) TcCLB.507211.40; TcCLB.511351.9; XPRT; GMP synthase: TcCLB.508085.10; GMP reductase; TcCLB.506519.130). In contrast, enzymes associated with the adenine branch are preferentially expressed in trypomastigotes over amastigotes: eg hypoxanthine-guanine phosphoribosyltransferase: TcCLB.506457.30; adenine phosphoribosyltransferase: TcCLB.508207.74; adenylsuccinate synthetase: TcCLB.508731.60). This observation raises the possibility that flux through the purine salvage pathway is tuned to the different environments encountered by *T. cruzi* life stages.

The anticipated demand for lipid precursors to support membrane synthesis in *T. cruzi* amastigotes is mirrored by the enrichment of GO functions associated with isoprenoid (GO:0008299), sterol (GO:0006696) and fatty acid (GO:0006633) synthesis at early stages of amastigote development (S9 Table). Specifically, several enzymes in the mevalonate pathway are upregulated (Fig 2A) as are the first two enzymes in the fatty acid synthesis/elongation
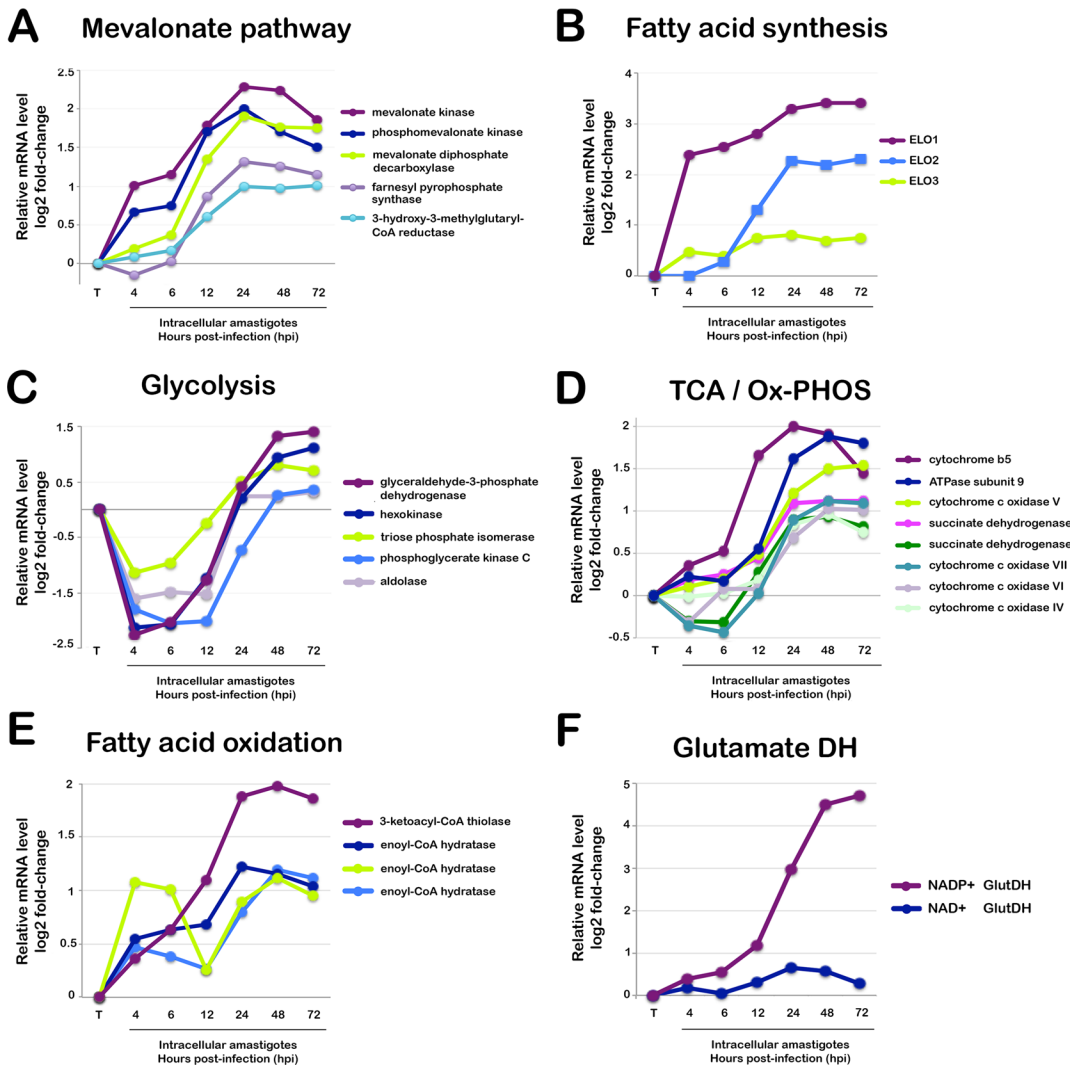

Fig 2. Temporal expression of metabolic pathway genes in mammalian-infective stages of *T. cruzi*. Relative mRNA expression of selected genes in intracellular *T. cruzi* amastigote stages (4–72 hpi) compared to extracellular trypomastigotes (**T**). Genes in the following metabolic pathways are highlighted: (**A**) **Mevalonate pathway**: mevalonate kinase (TcCLB.436521.9), mevalonate diphosphate decarboxylase (TcCLB.507993.330), squalene monooxygenase (TcCLB.509589.20), farnesyl pyrophosphate synthase (TcCLB.508323.9), 3-hydroxy-3-methylglutaryl-CoA reductase (TcCLB.509167.20). (**B**) **Fatty Acid Synthesis:** fatty acid elongase 1 (ELO1) (TcCLB.506661.30), fatty acid elongase 2 (ELO2) (TcCLB.506661.20), fatty acid elongase 3 (ELO3) (TcCLB.506661.10). (**C**) **Glycolysis:** glyceraldehyde-3-phosphate dehydrogenase (TcCLB.506943.60); hexokinase (TcCLB.508951.20), triosephosphate isomerase (TcCLB.508647.200), phosphoglycerate kinase (TcCLB.511419.40), aldolase (TcCLB.504163.40). (**D**) **Tricarboxylic Acid / Oxidative Phosphorylation (TCA/Ox-PHOS):** cytochrome b5 (TcCLB.506773.44), ATPase subunit 9 (TcCLB.503579.70), cytochrome c oxidase subunit V (TcCLB.510565.30), succinate dehydrogenase 11 (TcCLB.504035.84), succinate dehydrogenase 6 (TcCLB.507091.30), cytochrome c oxidase subunit VII (TcCLB.509233.150), cytochrome c oxidase subunit VI (TcCLB.511145.10), cytochrome c oxidase subunit IV (TcCLB.506529.360). (**E**) **Fatty Acid Oxidation:** 3-ketoacyl-CoA thiolase (TcCLB.510507.20), enoyl-CoA hydratase/isomerase (TcCLB.511529.170); enoyl-CoA hydratase, mitochondrial (TcCLB.508185.10) enoyl-CoA hydratase/isomerase (TcCLB.510997.40). (**F**) **Glutamate Dehydrogenases (DH):** NADP+-GlutDH (TcCLB.507875.20), NAD+ GlutDH (TcCLB.509445.39). All values are reported as log2 fold-change of difference between expression at in the trypomastigote stage and intracellular stages as reported in S5 Table.

doi:10.1371/journal.ppat.1005511.g002

pathway [67] ELO1 (TcCLB.506661.30) and ELO2 (TcCLB.506661.20) (Fig 2B and S5 Table). Combined, these observations indicate that intracellular *T. cruzi* amastigotes generate sterols and fatty acids *de novo* to support replication and membrane homeostasis. Despite its biosynthetic capacity, *T. cruzi* may opt to scavenge some lipids or precursors from its host cell as seen with other parasites [68–70]. It is currently unclear if or how *T. cruzi* amastigotes balance *de novo* synthesis of macromolecular precursors with uptake from the host cell.

Metabolic adaptation during intracellular *T. cruzi* development

Intermediary metabolism has been of interest to biochemists in the *T. cruzi* field for more than fifty years (e.g. [71, 72]). *T. cruzi*, like its trypanosomatid relatives, has a partially compartmentalized glycolytic pathway [73] and a non-canonical TCA cycle is predicted [74]. All major *T. cruzi* life stages exhibit the capacity for oxidative phosphorylation [75, 76]. Although developmental differences in energy metabolism have been documented for *T. cruzi* (e.g. [77, 78]), the specific impact of mammalian host cell colonization on parasite and host bioenergetics remains a poorly understood aspect of the host-parasite relationship. Here, we report dynamic changes in the expression of *T. cruzi* genes involved in energy metabolism as trypomastigotes establish intracellular infection in mammalian cells (Fig 3A). Highlighted are glycolytic enzymes (Fig 2C) and components of the mitochondrial electron transport chain (Fig 2D) that exhibit biphasic responses during infection. *T. cruzi* transcripts encoding glycolytic enzymes were rapidly repressed in nascent amastigotes as compared to trypomastigotes (4–12 hpi) consistent with an earlier report that intracellular amastigotes do not take up hexose sugars [79]. However, transcript levels corresponding to a subset of glycolytic genes rebound in mature *T. cruzi* amastigotes (Fig 2C), with the emergence of 'Glycolysis' as an enriched GO term (GO:0006096) at this stage (>24 hpi) as compared to immature amastigotes (eg. Ama4) (S9 Table) suggesting that replicative amastigote stages likely retain some capacity for glycolysis inside the mammalian host cell.

Genes encoding enzymes involved in mitochondrial oxidative phosphorylation are also upregulated in the intracellular replicative stages of *T. cruzi* as compared to trypomastigotes (Fig 2D; Fig 3A) suggesting that the respiratory capacity differs for these two parasite life stages. A mitochondrial stress test was performed to test this prediction. In line with early comparative studies of mitochondrial respiratory capacity in *T. cruzi* life cycle stages [75, 80], basal respiration (Fig 3B) and ATP-coupled respiration (Fig 3C) were found to be similar for trypomastigotes and amastigotes. In contrast, the bioenergetic properties of these two parasite life stages diverged significantly at the level of mitochondrial spare respiratory capacity (SRC) (Fig 3D), an indicator of the potential of a cell to respond to sudden increases in energy demand [81]. In repeated measurements, isolated intracellular amastigotes displayed measurable mitochondrial reserve capacity whereas trypomastigotes had none (Fig 3D). Furthermore, trypomastigotes failed to maintain ATP levels in the absence of exogenous carbon, whereas homeostatic mechanisms to preserve cellular ATP levels were evident in amastigotes (Fig 3E). We hypothesize that mitochondrial reserve capacity may be important for *T. cruzi* amastigotes in the context of cell/tissue infection to provide a buffer against environmental stressors such as oxidative stress (e.g. [82]). A key short-term regulator of spare respiratory capacity in cells is cytochrome c oxidase (mitochondrial complex IV) [83]. Several cytochrome c oxidase subunits are more highly expressed at the transcript level in mature amastigotes as compared to trypomastigotes (Fig 2D and S5 Table). Differences in expression of this enzyme complex may contribute to observed homeostatic differences and mitochondrial SRC between these life stages. In the related organisms, *T. brucei* and *Leishmania*, cytochrome c oxidase subunit expression correlates with mitochondrial respiration rates, ATP production, parasite replication and virulence [84–86]. In this
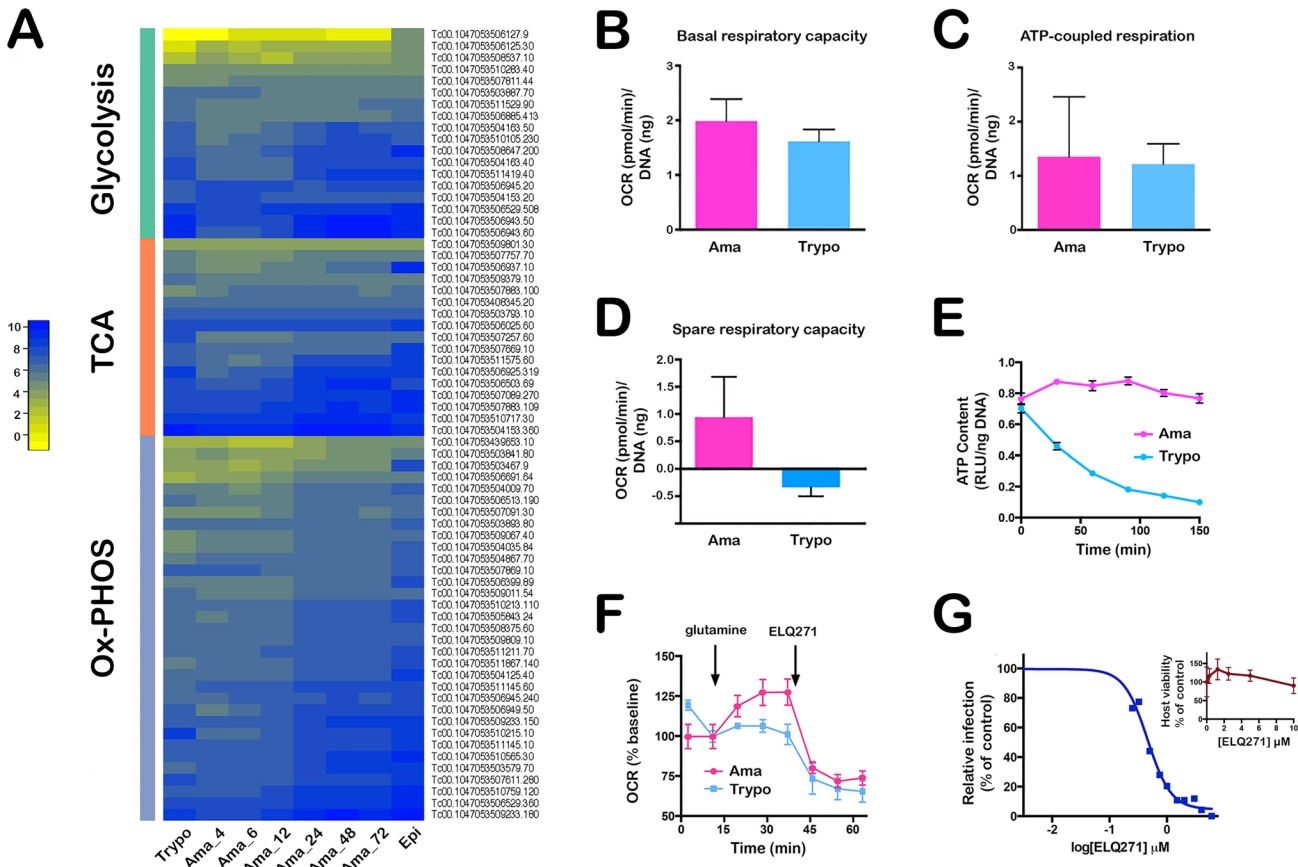
Fig 3. Validation of predicted metabolic features of *T. cruzi* developmental stages. (A) Heatmap of expression values of annotated *T. cruzi* genes predicted to function in intermediary metabolism with a focus on glycolysis, TCA cycle and Ox-PHOS. **(B)** Calculated basal respiratory capacity **(C)** ATP-linked respiration and **(D)** spare-respiratory capacity of extracellular trypomastigotes and isolated intracellular amastigotes (60 hpi) as pmol of oxygen consumed per min (oxygen consumption rate; OCR) normalized to *T. cruzi* DNA (ng) per well. **(E)** ATP content measured in isolated trypomastigotes and amastigotes in KHB buffer without a consumable carbon source at time points indicated. **(F)** OCR response to glutamine (10 mM) and ELQ271 (10 μM) in isolated *T. cruzi* trypomastigotes and amastigotes. **(G)** Dose-dependent inhibition of *T. cruzi* amastigote growth in HFF following addition of ELQ271 at 18 hpi and relative infection measured at 72 hpi. Host cell viability and growth (inset) is unaffected by the compound over the course of the assay. Graphs shown are representative of 3 independent experiments.

doi:10.1371/journal.ppat.1005511.g003

light, it would be interesting to probe the relationship between cytochrome c oxidase activity, mitochondrial spare respiratory capacity and *T. cruzi* strain-dependent differences in host infectivity and virulence.

The main carbon sources that fuel energy production in intracellular *T. cruzi* amastigotes are not definitively known. It is assumed that glucose is limiting in the host cell cytosol and that intracellular amastigotes rely on uptake of amino acids and fatty acids for energy [42, 87]. Our transcriptomic data generally support this projected trend with the anticipated increase in expression of fatty acid oxidation genes (Fig 2E) and of several amino acid permeases (S5 and S10 and S8 Fig cluster 5) during amastigote development in mammalian cells. In addition, glutamate dehydrogenase (GlutDH) was found to be highly expressed in replicative *T. cruzi* amastigote stages as compared to trypomastigotes (Fig 2F and S5 Table). GlutDH exerts an important anaplerotic function by converting glutamate to α-ketoglutarate that feeds into the TCA cycle to replenish intermediates diverted to biosynthetic functions. *T. cruzi* has two different glutamate dehydrogenase activities: one NAD+-linked [88] and the other NADP+-linked [89]. Both activities are expressed in epimastigotes [90]; also reflected in our mRNA expression

analysis (S5 Table). However, only the NADP+-linked enzyme (TcCLB.507875.20) is upregulated in intracellular amastigotes (Fig 2F). The significance of this finding is unknown but suggests a degree of specialization for these enzymes in the two main replicative *T. cruzi* life stages. Consistent with higher GlutDH expression in *T. cruzi* amastigotes, we find that exogenous glutamine drove higher oxygen consumption rates (OCR) in isolated amastigotes as compared to trypomastigotes (Fig 3F). Oxidative phosphorylation is inhibited in both parasite life cycle stages by ELQ271 (Fig 3F), an endochin-like quinolone that selectively inhibits mitochondrial complex III activity of apicomplexan parasites over mammalian cells [91–93]. We further show that intracellular *T. cruzi* amastigote growth is inhibited by ELQ271 in a dose-dependent manner (Fig 3G), whereas growth/viability of human fibroblast host cells is not compromised (Fig 3G; insert) as expected [91–93]. Although it is well-established that mitochondrial respiration in *T. cruzi* is sensitive to the mammalian complex III inhibitor, antimycin A [75] this is the first demonstration of sensitivity of a kinetoplastid protozoan to endochin-like quinolones. These data agree with the recent demonstration that electron transport is a targetable process in intracellular *T. cruzi* [94] and support the concept that mitochondrial respiratory chain activity may be essential for *T. cruzi* amastigote proliferation in mammalian cells.

As an obligate intracellular *T. cruzi* life cycle stage, amastigotes must tap into the nutritional resources of their mammalian host cells in order to survive. The ability of *T. cruzi* to colonize a wide variety of mammalian cell types suggests a high degree of metabolic flexibility and the capacity for rapid adaptation. With the exception of the essential nutrients that *T. cruzi* is incapable of synthesizing (eg. purines, pterins) we have little knowledge of what cytosolically-localized *T. cruzi* amastigotes extract from their host cells or how energy metabolism is balanced in this parasite life cycle stage. While isotopic tracer experiments are required to make any definitive statements regarding nutrient uptake and utilization by intracellular *T. cruzi* amastigotes, the dynamic changes observed for core metabolic processes at the transcriptome level is indicative of metabolic remodeling during *T. cruzi* amastigote development. Similar metabolic retooling has been described in related kinetoplastid protozoan parasites [95–99]. Going forward, it will be critical to understand how *T. cruzi* amastigote metabolism is wired, how it is couples to host metabolic pathways, the degree of flexibility that exists within these connections and how this can change in the context of the different cell types that *T. cruzi* colonizes in the human host.

Host cell response to *T. cruzi* infection

Transcriptomic changes induced in mammalian host cells by *T. cruzi* have been reported in a variety of host cell types and under different experimental conditions [100–110]. Because *T. cruzi* is capable of infecting most nucleated mammalian cell types, there has been little consistency among these experiments, complicating direct comparison of host transcriptional response data. Here we opted to use human foreskin fibroblasts (HFF) as the model host cell type for *T. cruzi* infection to facilitate comparisons to microarray hybridization studies previously conducted by our group [100, 107]. As outlined in the Methods section, our experimental approach permitted the capture of both parasite and host transcriptome response information across an infection time course *in vitro* (Fig 1A). RNA-Seq libraries generated in parallel for mock-infected HFF cultures provided the appropriate controls for each infection time point. As anticipated, some of the previously documented features of the global host transcriptional response to *T. cruzi* infection [100, 107] were recapitulated in the present analysis (S7 Table) as discussed below. One notable difference, however, relates to the detection of ~450 differentially expressed genes in *T. cruzi*-infected fibroblasts within the first 4 hpi of infection (S4 Table) contrasting sharply with the minimal response previously observed at early parasite infection

time points [100]. The enhanced detection capability is likely due to the increased dynamic range and sensitivity achieved with the deep sequencing approach used here.

The Gene Ontology enrichment categories associated with the early transcriptome response in *T. cruzi* infected fibroblasts (4–6 hpi), while numerous (S10 Table), can be distilled into two main categories: host cell cycle progression and immune response. Among the 288 fibroblast genes that are upregulated ≥2-fold following parasite infection at 4 hpi (S4 and S7 Tables) a significant enrichment in functions related to cell cycle progression, mitosis and cell division are observed eg. GO:0000278 (S10 Table; upregulated). Plotting the mRNA expression dynamics for several cell cycle regulators (Fig 4A) shows this trend continuing until 24 hpi, after which the expression of host cell cycle genes declines precipitously (Fig 4A, S8B Fig cluster 2, and S12 Table) such that 'mitotic cell cycle' becomes an enriched biological process associated with downregulated host genes (S10 Table; downregulated). Overall, these observations coincide with our previous finding that *T. cruzi* infection pushes host cells toward S-phase in the first 24 hr of the infection cycle, with a subsequent block imposed on host cell cytokinesis at later time points [107].
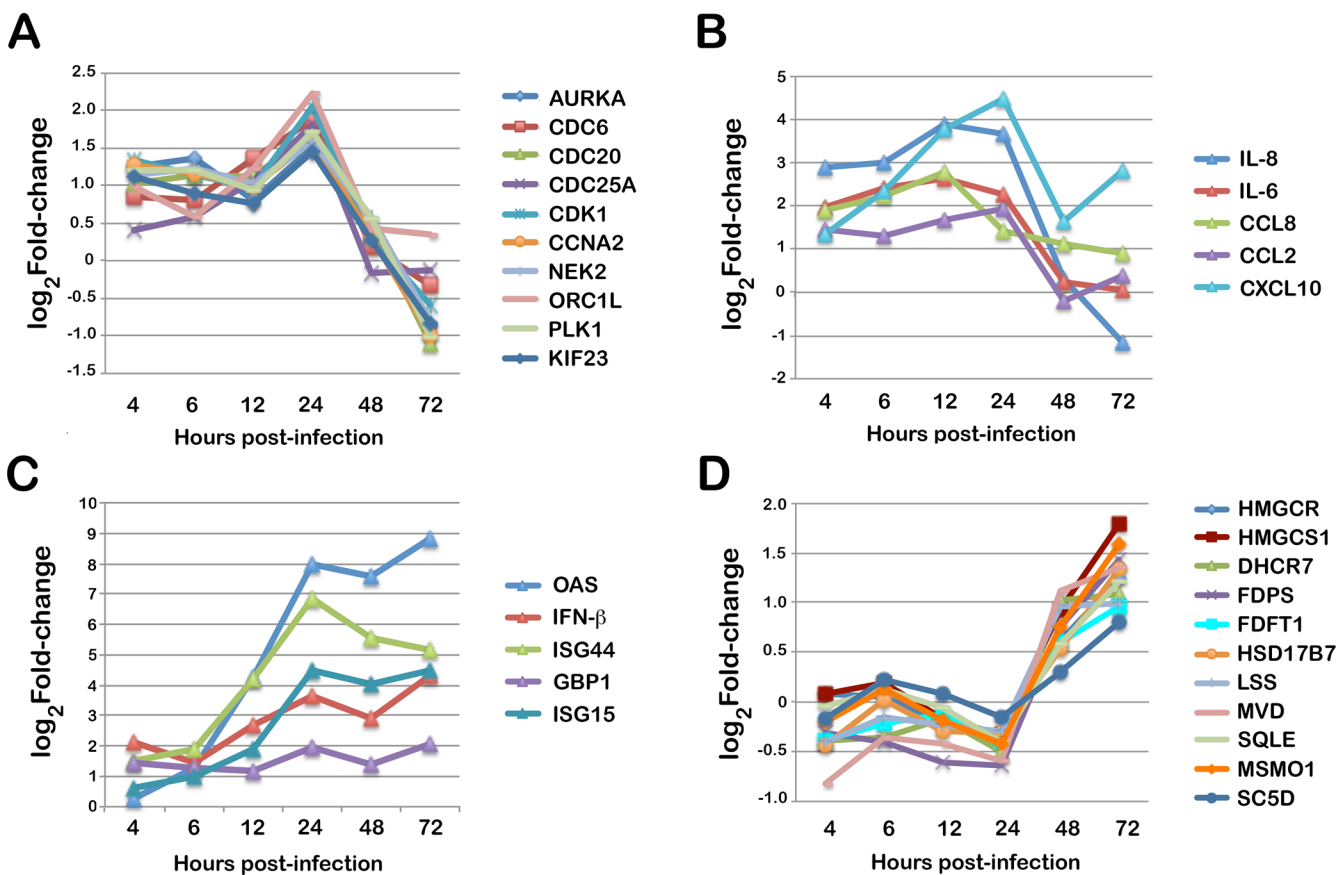
Fig 4. Dynamic host response signatures in *T. cruzi*-infected human fibroblasts. Expression patterns for selected genes in the most strongly modulated pathways in *T. cruzi* infected HFF. Genes in the following categories are highlighted. **(C) Mitotic Cell cycle:** *AURKA* (ENSG00000087586); *CDC6* (ENSG00000094804); *CDC20* (ENSG00000117399); *CDC25A* (ENSG00000164045); *CDK1* (ENSG00000170312); *CCNA2* (ENSG00000145386); *NEK2* (ENSG00000117650); *ORC1L* (ENSG00000085840); *PLK1* ENSG00000137807); KIF23 (ENSG00000137807). **(B) Cytokines/Chemokines:** *IL-8* (ENSG00000169429); *IL-6* (ENSG00000136244); *CCL8* (ENSG00000108700); *CCL2* (ENSG00000108691); *CXCL10* (ENSG00000169245). **(C) Type I Interferon:** *OAS* (ENSG00000089127); *IFNB* (ENSG00000171855); *ISG44* (ENSG00000137959); *GBP1* (ENSG00000117228); *ISG15* (ENSG00000187608). **(D) Mevalonate/Sterol biosynthesis:** *HMGCR* (ENSG00000113161); *HMGCS1* (ENSG00000112972); *DHCR7* (ENSG00000172893); *FDPS* (ENSG00000160752); *FDFT1* (ENSG00000079459); *HSD17B7* (ENSG00000132196); *LSS* (ENSG00000160285); *MVD* (ENSG00000167508); *SQLE* (ENSG00000104549); *MSMO1* (ENSG00000052802); *SC5D* (ENSG00000109929). All values are reported as log2 fold-change of the difference in expression of infected and matched uninfected controls at each time point as listed in S7 Table.

doi:10.1371/journal.ppat.1005511.g004

An innate immune response to *T. cruzi* infection was also evident in the early transcriptome signature of infected fibroblasts (S10 Table; upregulated; e.g. GO:0002376) with the upregulation of pro-inflammatory cytokine and chemokine genes (Fig 4B and S7 Table) as well as type I interferon inducible genes (Fig 4C and S7 Table) with different dynamics (Fig 4C). Cytokine/chemokine gene expression peaks at 24 hpi (Fig 4B) whereas the type I IFN response (ie. genes that are expressed downstream of type I IFN receptor activation) increases gradually over the infection time course (Fig 4C) to become the dominant host transcriptomic signature by 72 hpi (S10 Table; upregulated). Differences in the expression profiles of these distinct immune response pathways is presumably related to differences in the mechanism of pathway activation by *T. cruzi* [111–116] and regulatory processes related to signal amplification [107]. Pro-inflammatory cytokine activation via Toll-like receptor (TLR) and cell-intrinsic response pathways is required for host protection against *T. cruzi* [111, 113–116]. In contrast, the type I IFN response does not require TLRs for activation in response to *T. cruzi* [112] and is associated with exacerbation of *T. cruzi* infection under instances of high parasite load to the detriment of the host [117], similar to the impact of type I IFNs on the host in a number of other non-viral pathogen infection models (reviewed in [118]). Although not required for host protection, type I IFN (*IFNA6*) and several IFN-inducible genes (*IFI44L*, *STAT1* and *GBP1*) emerged in an unbiased RNAi screen conducted in HeLa cells [119] as positively effecting the *T. cruzi* infection process. This finding raises the unexplored possibility that the host type I IFN response triggered by *T. cruzi* may be beneficial to the parasite under certain circumstances.

Corresponding with increasing intracellular parasite burden is the elevated expression of host genes related to metabolism. Included in this list are several classes of solute transporter (S7 Table) and enzymes involved in lipid biosynthesis (S8B Fig; cluster 4). In fact, most of the genes in the mevalonate pathway are upregulated $\geq$2-fold between 24–72 hpi (Fig 4D) as is *SREBP2* (ENSG00000198911), an important regulator cholesterol homeostasis in mammalian cells [120]. It is tempting to speculate that elevated sterol biosynthesis fuels membrane synthesis in infected host cells to accommodate a steadily increasing intracellular parasite load and/or provides a pool of sterol intermediates to be scavenged by intracellular amastigotes. However, given that cholesterol biosynthesis is an intensely oxygen-consuming process [121], it is possible that the main function of this late host response to *T. cruzi* is defense against oxidative stress. While the presence of replicating parasites in the host cell cytoplasm is expected to dramatically impact energy homeostasis in the host cell, energy metabolism does not emerge as an enriched GO function at any time in the intracellular infection cycle (S12 Table). Thus, the cellular response to such perturbations is predicted to occur at the post-transcriptional and post-translational levels.

The ability to simultaneously capture host cell and parasite transcriptomes with high resolution and sensitivity sets the stage for the generation of host-parasite interaction networks. The integration of transcriptome data with other types of expression data and with functional information will be instrumental in modeling the critical aspects of the parasite-host interaction and aid in the identification of targetable processes therein. As a limited exercise, we performed an intersection of datasets containing host genes that are upregulated in response to *T. cruzi* infection (24 hpi; S7 Table) with those previously shown to impact *T. cruzi* growth in a genome-scale RNAi screen [119]. Within this subset of genes (S13 Table) is *GCH1*, which encodes GTP-cyclohydrolase 1, the rate-limiting enzyme in tetrahydrobiopterin (BH$_4$) synthesis. In previous work we demonstrated that siRNA-mediated knockdown of *GCH1* expression in host cells impaired intracellular *T. cruzi* amastigote growth in a manner that was rescued by the addition of dihydrobiopterin [119]. Here we find that *GCH1* (ENSG00000131979) is upregulated in *T. cruzi*-infected fibroblasts (S7 Table; $\geq$12 hpi) at the same time that its negative regulator (GCHI feedback regulator; ENSG00000137880) is repressed (S7 Table). Additionally,

the *T. cruzi* gene encoding pterin-4-alpha-carbinolamine dehydratase (PCDB1: TcCLB.503613.40), an enzyme involved in biopterin recycling, was also found to be rapidly upregulated in developing intracellular amastigotes (S5 Table; 4 hpi). Together, these observations are consistent with a predicted need to increase flux through the host BH_4 synthesis pathway to fuel the growth of intracellular *T. cruzi*, a pterin auxotroph [122]. With this example, it is possible to see how threads of a functional host-parasite network can emerge from data integration, an important goal of host-pathogen transcriptomic studies going forward.

Conclusion

A key feature of our work is the demonstrated ability to parse out human and parasite sequence reads from complex pools generated from *T. cruzi*-infected cells and to obtain high coverage of both the parasite and host transcriptomes to enable downstream analyses with high statistical confidence. As emphasized here, the simultaneous capture of dynamic changes in host and parasite gene expression over an infection time course provides immediate and new insights into the biology of *T. cruzi* infection and serves as a unique resource for the construction of high-resolution maps of parasite-host interactions. Moreover, the transcriptome dynamics observed during a major life stage transition in *T. cruzi* revealed marked similarities between this parasite and its trypanosomatid relatives with respect to the ordering of processes that control global gene expression during differentiation. Specifically, our data support previous observations in *T. brucei* [12, 48] and *Leishmania donovani* [11, 13, 23, 123] indicating that regulation of mRNA levels exerts the greatest impact during the initial phases of a developmental transition in these parasites, whereas downstream mechanisms such as translational efficiency and post-translational modification dominate in the subsequent phases of development and maintenance. While regulation of gene expression in *T. cruzi* is understood to be multi-layered and complex (eg. [124, 125]), with translational efficiency playing a key regulatory role [18], our findings argue for the value of transcriptome data to derive meaningful biological inferences related to parasite biology. Extrapolation of this finding to the many hypothetical genes encoded in the *T. cruzi* genome, for which we now have dynamic mRNA expression data, has exciting implications for biological discovery in the trypanosome field. Finally, integration of transcriptome information, with emerging proteomic (eg. [87, 126–133]), functional [119] and metabolic data will, in the near future, create novel opportunities to pinpoint critical processes that govern successful pathogen colonization in the host with links to Chagas disease pathogenesis and increase the potential to identify novel targets for this important neglected disease.

Methods

Parasite maintenance and mammalian cell infection

Trypanosoma cruzi Y strain [134] was cultivated by weekly passage in $LLcMK_2$ cells (ATCC #CCL-7) in Dulbecco's modified Eagle medium (DMEM) with 2% fetal bovine serum (FBS), 2 mM L-glutamine, 10 mM HEPES and penicillin-streptomycin maintained at 37°C and 5% CO_2. *T. cruzi* trypomastigotes released into the supernatants of infected $LLcMK_2$ cells were collected, pelleted by centrifugation (1000*g*, 10 min) and collected from the supernatant after swimming up from the pellet over a 2–4 hour incubation at 37°C, 5% CO_2. Human foreskin fibroblasts (HFF) (ATCC #CRL-2522) were seeded onto 10 cm^2 plates or T-25 flasks in complete DMEM (as above, with 10% FBS) and grown to 80% confluence (48 hr) before infection. Briefly, HFF monolayers were washed with DMEM-2%FBS (DMEM-2) and either incubated with medium (mock) or *T. cruzi* trypomastigotes for 2h before washing 5 times with PBS and incubation in DMEM-2 at 37°C and 5% CO_2. At the indicated time points (4–72 hpi), cells

were rinsed with ice-cold PBS and lysed directly in Trizol for RNA isolation. *T. cruzi* epimastigotes, maintained at mid-log phase in liver infusion tryptose medium at 27°C, or purified extracellular trypomastigotes (>95% pure) were also used for RNA isolation. To obtain intracellular *T. cruzi* amastigotes for metabolic studies, infected LLcMK$_2$ (60 hpi) were washed with ice-cold Krebs-Henseleit Buffer (KHB) containing 0.5mM glucose, and scraped into 1ml ice-cold KHB + 0.5mM glucose with a cell scraper. Dislodged cells were collected in 9ml final volume of KHB + 0.5mM glucose in a 50ml tube, and centrifuged at 2100g for 10 minutes at 4°C. Pelleted cells were resuspended in 1ml of KHB + 0.5mM glucose, transferred to Eppendorf tubes, vortexed for 45s and passed through a 1ml syringe with a 28.5G needle 20 times to release amastigotes. Unbroken cells and debris were pelleted at 100g for 1 minute and the amastigote-enriched supernatant was pelleted at 1000g for 10 minutes at room temperature. Amastigotes were resuspended in warm (37°C) KHB + 0.5mM glucose at $2x10^7$ amastigotes per ml.

RNA isolation and library construction for simultaneous transcriptome profiling of parasite and host cells

RNA was isolated in Trizol reagent, as per manufacturer, and the quality determined using an Agilent 2100 bioanalyzer and quantified by qPCR using a KAPA Biosystems library quantification kit. Standard Illumina protocols were used for mRNA-Seq sample preparation. RNA-Seq libraries were constructed from polyA-enriched mRNAs generated from eight *T. cruzi* developmental stages: epimastigotes, trypomastigotes, and intracellular amastigotes at 4, 6, 12, 24, 48 and 72 hrs post-infection (hpi) of HFF. Libraries were also constructed from mock-infected HFF at the same time points. For each condition, 2–4 independent biological replicates were sequenced on an Illumina HiSeq1000. A total of 2.7 billion reads from 35 samples were generated from 101 bp paired-ends.

Sequence read processing, alignment, abundance estimation and data normalization

The quality of the raw reads was evaluated using the FastQC tool [http://www.bioinformatics.babraham.ac.uk/projects/fastqc/] and one nucleotide was trimmed using the FASTX toolkit (Hannon Lab, CSHL) when the mean of the quality score fell below 30 in the last position (see analysis pipeline S1 Table). Tophat v2.0.8 [36] was used to align all reads to the reference human genome sequence (hg19, GRCh37) and independently to the of the *T. cruzi* CL Brener reference genome (v. 4.1) [35] Esmeraldo haplotype obtained from the TriTrypDB database (www.tritrypdb.org). Alignment settings allowed 2 mismatches per read and the default -g/—max-multihits parameter of -g = 20 was used for alignments to the human genome. A parameter of -g = 1 was used for *T. cruzi* to allow reads to map to a single locus in this organism where multi-gene families are abundant. The read counts per coding sequence (CDS) were determined using HTSeq [http://www-huber.embl.de/users/anders/HTSeq/] as listed *T. cruzi* (S2 Table) and human (S3 Table) genes.

Data quality assessment by statistical sampling and visualization

Weakly expressed genes, defined as having less than 1 read per million in 'n' of the samples, where 'n' is the size of the smallest group of replicates [135] (here n = 2 and 3 for the *T. cruzi* and human samples, respectively) were removed from subsequent analyses. Pearson correlation and standardized median correlation analyses, box plots, Principal Component Analysis (PCA) and Euclidean distances-based hierarchical clustering approaches were used to evaluate

replicates and the relationships between samples across time points and to visualize sample-sample distances. All components of our statistical pipeline, named cbcbSEQ, can be accessed on GitHub (https://github.com/kokrah/cbcbSEQ/). Samples that did not pass the following quality assessment procedure were removed: for each sample we computed the median pairwise correlation (mpc) to all other samples in the dataset (S5 Fig). A standard outlier identification method was then applied to remove samples with low correlation to the other samples: samples were removed if their median pairwise correlation (mpc) is less than Q1(mpc)– 1.5 IQR(mpc) where Q1(mpc) and IQR(mpc) are the first quartile and inter-quartile range of the median pairwise correlation across all samples respectively. HPGL0111 was removed from subsequent analyses as a result.

Differential expression analysis

A quantile normalization scheme was applied to all samples [86]. Following log2 transformation of the data, LIMMA [136] was employed for differential expression analyses. LIMMA utilizes a standard variance moderated across all genes using a Bayesian model and produces *p*-values with greater degrees of freedom [137]. When appropriate, the Voom module was used to transform the data based on observational level weights derived from the mean-variance relationship. Experimental batch effects were adjusted by including experimental batch as a covariate in our statistical model. Type I error introduced by multiple testing was corrected with q-value [138]. A contrast matrix was used within LIMMA. To control for expression profile changes in human cells that occur naturally over time in cell culture, normalized-log2-transformed expression values for each gene in 'uninfected' was subtracted from 'infected' in the paired uninfected/infected HFF samples at each time point. Differentially expressed genes were defined as genes with q-value < 0.05.

Filtering *T. cruzi* DEG lists to remove paralogous genes

Each list of differentially expressed *T. cruzi* genes generated from pairwise comparisons (S5 Table) was submitted to a search against itself using FASTA36 [139]. Groups of genes were counted as paralogous when observed with an e-value ≤0.0001 and percentage identity ≥80%. The first lexically listed gene in each group was taken as a representative for the group shown in S6 Table. It should be noted that while a large proportion of paralogous genes have been collapsed, a number of truncated (partial) genes as well as genes encoding large hypervariable regions (i.e. MASP) can only be manually removed, a process more prone to error due to reliance on manual curation.

K-means clustering and functional enrichment analysis

K-means clustering analysis was performed to identify genes with similar expression profiles across different developmental stages of *T. cruzi* or human host cells with the R function "kmeans" and using the Hartigan-Wong algorithm. Quantile-normalized and batch effect-adjusted expression values were used for clustering and Euclidean distance was computed as the distance metric; 8 partitions were used to generate the clusters following the method of [41, 140]. Lists of significantly regulated genes resulting from differential expression or clustering analyses were classified into GO functional categories and tested for enrichment using GOSeq, which applies Wallenius approximation to correct the bias of over-detection of differential expression for long and highly expressed transcripts [40]. False discovery rate (FDR) was controlled using the Benjamini and Hochberg's procedure [141].

Metabolic analyses

Mitochondrial respiratory capacity was measured using an XF^{e}24 extracellular flux analyzer (Seahorse Biosciences). Briefly, XF^{e}24 assay plates were pre-coated with 30 μl of 7.7% Cell-Tak (Corning) in 100 mM sodium bicarbonate, pH 8 for 30 minutes, then the wells were washed three times with 0.5 ml warm Krebs-Henseleit Buffer (KHB) before plating parasites. Isolated *T. cruzi* (Tulahuen strain) [142] trypomastigotes and amastigotes were resuspended in either XF Base Medium (Seahorse Biosciences) + 10mM glucose, 2mM glutamine, and 1mM sodium pyruvate or KHB + 0.5mM glucose at $2x10^7$ parasites/ml. $2x10^6$ parasites in 100 μl were delivered to each well of a Cell-Tak pre-coated Seahorse XF^{e}24 assay plate and immediately centrifuged at 2056g for 2 minutes. The volume of medium in each well was adjusted to a total volume of 450 μl/well of plating medium. To determine basal respiratory capacity, ATP-coupled respiration, and spare respiratory capacity, drugs from the XF Cell Mito Stress Test Kit (Seahorse Biosciences) were resuspended in warm media and injected at 10x their final well concentrations of 2.5μM oligomycin, 3μM carbonyl cyanide-4-(trifluoromethoxy)phenylhydrazone (FCCP), and a mixture of 1μM antimycin A and rotenone, in order. Results were normalized to parasite DNA based on a quantitative PCR assay of the single copy *T. cruzi* gene: OSBP (TcCLB.508211.10). At the end of the run, the media was replaced with 200 μl PBS and the plate was frozen at -20°C. DNA was isolated after thawing the plate using the DNeasy Blood and Tissue Kit (Qiagen). For qPCR, 10 μl of iTaq Universal SYBR Green Supermix (BioRad) was combined with 0.33 μl isolated DNA, 1 pmol each of primers to amplify a single copy *T. cruzi* gene OSBP (F: 5'-CAT CAC CTA CGG CCA CAA GA-3', R: 5'-TGC AGT GGA TAC GCA TAC GG-3'), and water for a 20 μl reaction volume. The reaction was run at 95°C for 5 minutes, then cycled 45 times at 95°C for 15 seconds followed by 60°C for 60 seconds. The amount of DNA per Seahorse plate well was calculated by comparing Ct values to a standard curve generated by 1:2 dilutions of 10 ng of *T. cruzi* DNA. To calculate basal respiratory capacity, the normalized oxygen consumption rates (OCR) after antimycin A and rotenone addition was subtracted from the baseline OCR. For ATP-coupled respiration, normalized OCR after oligomycin injection was subtracted from baseline OCR. Spare respiratory capacity was calculated as the difference between normalized OCR after FCCP injection and control wells at the same timepoint without any drug injections. Glutamine (Gibco, Life Technologies) and ELQ271 (generously supplied by M. Riscoe; OHSU) were resuspended in warm medium and injected at 10x their final well concentrations of 2mM and 10μM, respectively.

Total ATP determination

To measure total ATP levels, *T. cruzi* trypomastigotes and amastigotes were isolated (as above) and resuspended in Krebs-Henseleit Buffer (KHB) at $4x10^6$ parasites/ml. Trypomastigotes and amastigotes were plated at $4x10^5$ parasites in 100μl in a separate white 96-well plates (Corning) for each time point and incubated at 37°C. Parasites were lysed and ATP levels were determined using the ATPlite assay kit (PerkinElmer), measuring luminescence on a Varioskan Flash plate reader (ThermoScientific).

Drug susceptibility assay

HFF were seeded at 1500 cells/well in 384 well black bottom plates (Corning). At 24h post plating, cells were infected with β-galactosidase expressing *T. cruzi* Tulahuen strain (moi 5) for 2hr, washed twice, and left in DMEM (2% FCS, 2 mM glutamine, 1 mM pyruvate). At 18hpi cells were treated with 0.3–10 μM of ELQ271. At 72 hpi HFF viability was measured in a fluorescence-based readout (CellTiter-Fluor, Promega) and *T. cruzi* was measured by luminescence-based readout (Beta-Glo reagent, Promega) using an Envision Plate Reader

(PerkinElmer) as described [32]. The relative infection (RLU/RFU) was calculated and normalized to untreated control fitted by non-linear regression to high (= 100%) and low (= 0%) values using GraphPad Prism software.

Quantitative RT-PCR

RNA was isolated from purified *T. cruzi* trypomastigotes and from infected monolayers (at the indicated timepoints post infection) following cell lysis in Trizol reagent and purification using the PureLink RNA Mini Kit (Ambion). DNase-digested (Turbo DNase, Ambion) total RNA (1 μg) was converted to cDNA using the iScript (Bio-Rad) cDNA synthesis kit according to manufacturer's instructions. Specific primer pairs to amplify genes of interest in quantitative-RT-PCR reactions were selected on their ability to form single peak in melting curve analysis and verified by sequencing of PCR products. Forward (F) and reverse (R) primer pairs for are listed below in a 5' to 3' orientation. Cation transporter (TriTrypDB: TcCLB.509197.39) F: GAGTGTCATGCTTGAAGTG and R: CGTTAAAAATAAGAGAAAATG; Glutamate dehydrogenase (TriTrypDB: TcCLB.507875.20) F: GAGTACTGCCAGGATTCTC and R: CAAA GCCAAGAAACTTAAG; Fatty acid elongase (TriTrypDB: TcCLB.506661.30) F: GAGGCAA CCTGCACATTTAAC and R: GTGTCCATCAACTCAGGAATCT; Fatty acid desaturase (TriTrypDB: TcCLB.511073.10) F: AAGGAACGTGAAGAATCTC and R: AACGGACTTCTCCA GATC; Hypothetical protein, conserved (TriTrypDB: TcCLB.509767.170) F: ATGAAGCTT GCGTTCTCT and R: GGTCACAATAGCCCAGTC; Ribosomal RNA large subunit gamma M1 (TriTrypDB: TcCLB.411483.20) F: TGTGGAAATGCGAAACAC and R: CCCAGGTTTTTG CTTTAATG. Relative mRNA transcript abundance was quantified by SYBR green (iTaq Universal SYBR Green Supermix, Bio-Rad) PCR using a StepOnePlus Real-Time PCR Systems (Applied Biosystems). Large subunit ribosomal RNA gamma (M1): TcCLB.411483.20) used as endogenous control.

Data accession

RNA-Seq data are available at the National Center for Biotechnology (NCBI) Sequence Read Archive (SRA) (http://www.ncbi.nlm.nih.gov/bioproject) under Bioproject PRJNA251582 (accession numbers ranging from SRR1346026-SRR1346052) and Bioproject PRJNA251583 (accession numbers ranging from SRR1346053-SRR1346059). Individual accession numbers are also shown in S1 Table.

Supporting Information

S1 Fig. Schematic of pipeline for differential expression analysis. The input/output for each step of the data processing and analysis is depicted in rectangular boxes. Software/scripts or methodological components are shown in italicized blue text. Decision-making steps are represented diamond-shaped boxes. The five stages to the analysis are shown in the left margin. The main figures or supplemental files in which data outputs from key steps in the pipeline can be found are highlighted in red.
(PDF)

S2 Fig. Distribution of global gene expression levels in all *T. cruzi* and human samples. For all samples from *T. cruzi* (**A**) intracellular and (**B**) extracellular stages, and (**C**) human, counts were normalized for sequencing library size and a box plot was generated to compare the distribution of per-gene counts (log2 counts per million with an offset of 1). The ends of the whiskers represent the lowest datum still within 1.5 interquartile range (IQR) of the lower quartile, and the highest datum still within 1.5 IQR of the upper quartile. Genes with extremely high or

low expression levels are shown as open circles above and below the whiskers, respectively. Mapped read counts from all parasite and human cell samples showed consistent degrees of dispersion as indicated by the nearly identical quartile distributions in similar samples. The median expression values for *T. cruzi* genes display a more compact distribution than that observed for the human genes.
(PDF)

S3 Fig. Heatmap of Pearson correlations. Gene counts were normalized for sequencing library size. All pairwise Pearson correlations were calculated and plotted as a heatmap to view the relatedness of samples and identify outliers for **(A)** *T. cruzi* and **(B)** human.
(PDF)

S4 Fig. Pairwise Pearson correlation between *T. cruzi* samples. Gene counts were normalized for sequencing library size. The Pearson correlation between each sample and all other samples was calculated and plotted to view the relatedness of samples and identify outliers.
(PDF)

S5 Fig. Pairwise Pearson correlation between human samples. Gene counts were normalized for sequencing library size. The Pearson correlation between each sample and all other samples was calculated and plotted to view the relatedness of samples and identify outliers.
(PDF)

S6 Fig. Standardized median Pearson correlation between *T. cruzi* and human samples. Gene counts were normalized for sequencing library size. The standardized median Pearson correlation between each sample and all other samples was plotted to view the relatedness of samples and identify outliers for **(A)** intracellular *T. cruzi*; **(B)** extracellular *T. cruzi* and **(C)** human samples. Letters in the sample name refer to experimental batch.
(PDF)

S7 Fig. Hierarchical clustering of *T. cruzi* and human samples. Hierarchical clustering analysis based on Euclidean distance was performed using all **(A)** *T. cruzi* or **(B)** Human genes after filtering for weakly expressed genes, quantile normalization, and inclusion of the batch variable in the statistical model used by **Limma**. Colors along the top of the heatmap indicate the developmental stage and colors along the left side of the heatmap indicate the batch/experimental date.
(PDF)

S8 Fig. K-means clustering of gene expression in *T. cruzi* and human cells during the course of infection. K-means clustering of genes from **(A)** *T. cruzi* and **(B)** human across the intracellular infection course were presented. Log2-transformed and quantile-normalized batch-adjusted gene expression values (y-axis) are plotted across the seven conditions (trypo, 4, 6, 12, 24, 48, 72 hpi) for *T. cruzi* and six time points for human (4, 6, 12, 24, 48, 72 hpi) on the x-axis. Genes included in each of the clusters are listed in <u>S11 Table</u> and <u>S12 Table</u>.
(PDF)

S9 Fig. Independent validation of selected developmentally regulated metabolic genes in *T. cruzi*. Expression of selected *T. cruzi* transcripts in intracellular infection stages (6–72 hr post-infection) relative to extracellular trypomastigotes (expression level arbitrarily set to 1). Data derived from RNA-Seq differential expression analysis **(A)** or qRT-PCR **(B)** is shown for the following *T. cruzi* (Y strain) genes: TcCLB.509197.39: Cation transporter (CAT); TcCLB.507875.20: glutamate dehydrogenase (GlutDH); TcCLB.508373.20: dihydroorotase (DHO); TcCLB.506661.30: fatty acid elongase (FAE); TcCLB.511073.10: fatty acid desaturase

(FAD) and TcCLB.509767.170: hypothetical protein (HYP). Error bars in (B) represent the mean of duplicate samples.
(PDF)

S10 Fig. Temporal expression of selected *T. cruzi* RNA-binding proteins and flagellum-associated genes. Relative mRNA levels of **(A)** *T. cruzi* RNA-binding proteins and **(B)** flagellar genes that were differentially expressed in at least one of the intracellular amastigote stages (4–72 hpi) as compared to extracellular trypomastigotes (**T**).
(PDF)

S1 Table. Samples collected and mapping statistics. Complete description of all samples included in this analysis, including sample ID, SRA accession number, developmental stage, infection status, experimental batch, trimming information, number of raw reads, and number and percentage of reads mapped to each reference genome.
(XLSX)

S2 Table. Raw mapped read counts and log-transformed quantile-normalized cpm expression values for *T. cruzi* genes. Tophat was used to align *T. cruzi* cDNA reads to align to the reference genome as described in Methods. The abundance of reads mapping to each coding sequence (CDS) was determined using HTSeq (Raw reads). Weakly expressed genes, defined as having less than 1 read per million in 'n' of the samples, where 'n' is the size of the smallest group of replicates (here n = 2) were removed from subsequent analyses. A quantile normalization scheme was applied to all samples. Following log2 transformation of the data, the count per million values (cpm) were calculated for each gene using in-house script. All components of our statistical pipeline, named cbcbSEQ, can be accessed on GitHub (https://github.com/kokrah/cbcbSEQ/).
(XLSX)

S3 Table. Raw mapped read counts and log-transformed quantile-normalized cpm expression values for human genes. Tophat was used to align human cDNA reads to align to the reference genome as described in Methods. The abundance of reads mapping to each coding sequence (CDS) was determined using HTSeq (Raw reads). Weakly expressed genes, defined as having less than 1 read per million in 'n' of the samples, where 'n' is the size of the smallest group of replicates (here n = 3) were removed from subsequent analyses. A quantile normalization scheme was applied to all samples. Following log2 transformation of the data, the count per million values (cpm) were calculated for each gene using in-house script. All components of our statistical pipeline, named cbcbSEQ, can be accessed on GitHub (https://github.com/kokrah/cbcbSEQ/).
(XLSX)

S4 Table. Summary of Differentially Expressed Genes (DEGs). The number of differentially expressed genes (DEG) obtained with Limma software with t-statistic for *T. cruzi* or human fibroblast expression data before and after imposing a $\geq$ 2-fold cut-off filter (abs(log$_2$FC) $\geq$ 1.0). *T. cruzi* DEG lists were further filtered to collapse paralogous genes to a single representative gene as described in the Methods.
(XLSX)

S5 Table. Report of differential expression analysis for *T. cruzi* genes. Each sheet reports differential expression results for a specific pairwise comparison. The columns include Gene ID, gene function, log2 fold change (FC), *P* value, q-value, adjusted *P* value, average expression value, qvals.fc, and adjPvals.fc. The latter two are Booleans set to 1 when abs(log$_2$ FC) $\geq$ 1.0 and q-value or adjusted *P* value < 0.05 respectively. Genes are considered differentially

expressed when the qvals.fc = 1.
(XLSX)

S6 Table. *T. cruzi* DEGs with paralogues collapsed. Differentially expressed genes from S5 Table were filtered to remove all but a single representative of each paralogous gene group. These filtered gene lists served as the starting point for k-means clustering and functional enrichment analyses.
(XLSX)

S7 Table. Report of differential expression analysis for human genes. Each sheet reports differential expression results for a specific comparison. The columns include gene id, gene function, log2 fold change, P value, q-value, adjusted P value, average expression value, qvals.fc, and adjPvals.fc. The latter two are Booleans set to 1 when $abs(\log_2 FC) \geq 1.0$ and q-value or adjusted P value < 0.05 respectively. Genes are considered differentially expressed when the qvals.fc = 1.
(XLSX)

S8 Table. Overrepresented *T. cruzi* genes by developmental stage. Each sheet contains a list of *T. cruzi* genes that are expressed at a significantly higher level ($\geq$2-fold difference in expression) in one parasite life cycle stage as compared with the other two life stages with amastigote transcriptome data from the 24 hpi infection time point serving as the representative amastigote sample.
(XLSX)

S9 Table. Enriched Gene Ontology terms in differentially expressed *T. cruzi* genes. The enriched Gene Ontology (GO) terms associated with the differentially expressed genes (DEG) emerging from pairwise comparisons of *T. cruzi* life stages (listed in S6 Table). Data are presented for each GO domain (biological process, molecular function, cellular component) in separate worksheets. GO term, total number of genes in the GO category, number of DEGs present within the category, P value for the relevant GO category over-represented among DEGs in the comparison, adjusted P value and description of the enriched GO category included.
(XLSX)

S10 Table. Enriched Gene Ontology terms in differentially expressed human genes. The enriched Gene Ontology (GO) terms associated with the differentially expressed genes (DEG) emerging from pairwise comparisons of human samples (listed S7 Table) DEG lists were filtered by collapsing paralogous gene families prior to conducting GO enrichment analysis. Data are presented for each GO domain (biological process, molecular function, cellular component) in separate worksheets with GO term, total number of genes in the GO category, number of DEGs present within the category, P value for the relevant GO category over-represented among DEGs in the comparison, adjusted P value and description of the enriched GO category included.
(XLSX)

S11 Table. Enriched Gene Ontology terms in *T. cruzi* gene clusters. Enriched Gene Ontology (GO) terms associated with K-means gene clusters of differentially expressed *T. cruzi* genes (shown in S8A Fig) over the course of a human fibroblast infection. Columns contain (A) Name of the K-means cluster corresponding to those in S8A Fig; (B) GO category; (C) Total number of genes in category; (D) Number of differentially expressed genes (DEG) in category; (E) P value for over-represented genes in category; (F) the adjusted P value and (G) Gene

ontology term.
(XLSX)

S12 Table. Enriched Gene Ontology terms in human gene clusters. Enriched Gene Ontology (GO) terms associated with K-means gene clusters of differentially expressed human fibroblast genes associated with a *T. cruzi* infection time course (shown in S8B Fig). Columns contain (A) Name of the K-means cluster corresponding to those in S8B Fig; (B) GO category; (C) Total number of genes in category; (D) Number of differentially expressed genes (DEG) in category; (E) *P* value for over-represented genes in category; (F) the adjusted *P* value and (G) Gene ontology term.
(XLS)

S13 Table. Intersection of host cell expression and functional datasets. List of human genes arising from the intersection of two datasets: **(1)** the set of human fibroblast genes that are upregulated in *T. cruzi* infected cells at 24 hpi (from S7 Table; 838 genes) and **(2)** the set of primary hits from a human genome-wide siRNA screen that were identified as permissive for *T. cruzi* infection [119] (382 genes).
(XLSX)

Acknowledgments

Author Contributions

Conceived and designed the experiments: NMES BAB. Performed the experiments: YL KLC JC PP DMN SSS. Analyzed the data: YL MRT KO ATB HCB NMES BAB. Wrote the paper: YL SSS KC NMES BAB.

References

1. Rassi A Jr., Rassi A, Marin-Neto JA. Chagas disease. Lancet. 2010; 375(9723):1388–402. doi: 10.1016/S0140-6736(10)60061-X PMID: 20399979

2. Tardieux I, Webster P, Ravesloot J, Boron W, Lunn JA, Heuser JE, et al. Lysosome recruitment and fusion are early events required for trypanosome invasion of mammalian cells. Cell. 1992; 71 (7):1117–30. PMID: 1473148

3. Tomlinson S, Vandekerckhove F, Frevert U, Nussenzweig V. The induction of Trypanosoma cruzi trypomastigote to amastigote transformation by low pH. Parasitology. 1995; 110 (Pt 5):547–54. PMID: 7541124

4. Ley V, Robbins ES, Nussenzweig V, Andrews NW. The exit of Trypanosoma cruzi from the phagosome is inhibited by raising the pH of acidic compartments. J Exp Med. 1990; 171(2):401–13. PMID: 2406362

5. Soll DR. The role of phenotypic switching in the basic biology and pathogenesis of Candida albicans. J Oral Microbiol. 2014; 6. doi: 10.3402/jom.v6.22993

6. Kafsack BF, Rovira-Graells N, Clark TG, Bancells C, Crowley VM, Campino SG, et al. A transcriptional switch underlies commitment to sexual development in malaria parasites. Nature. 2014; 507 (7491):248–52. doi: 10.1038/nature12920 PMID: 24572369

7. Johnson PJ, Kooter JM, Borst P. Inactivation of transcription by UV irradiation of T. brucei provides evidence for a multicistronic transcription unit including a VSG gene. Cell. 1987; 51(2):273–81. PMID: 3664637

8. Muhich ML, Boothroyd JC. Polycistronic transcripts in trypanosomes and their accumulation during heat shock: evidence for a precursor role in mRNA synthesis. Mol Cell Biol. 1988; 8(9):3837–46. PMID: 3221866

9. Tschudi C, Ullu E. Polygene transcripts are precursors to calmodulin mRNAs in trypanosomes. EMBO J. 1988; 7(2):455–63. PMID: 3366120

10. Ullu E, Matthews KR, Tschudi C. Temporal order of RNA-processing reactions in trypanosomes: rapid trans splicing precedes polyadenylation of newly synthesized tubulin transcripts. Mol Cell Biol. 1993; 13(1):720–5. PMID: 8417363

11. Rosenzweig D, Smith D, Myler PJ, Olafson RW, Zilberstein D. Post-translational modification of cellular proteins during Leishmania donovani differentiation. Proteomics. 2008; 8(9):1843–50. doi: 10. 1002/pmic.200701043 PMID: 18398879

12. Queiroz R, Benz C, Fellenberg K, Hoheisel JD, Clayton C. Transcriptome analysis of differentiating trypanosomes reveals the existence of multiple post-transcriptional regulons. BMC Genomics. 2009; 10:495. doi: 10.1186/1471-2164-10-495 PMID: 19857263

13. Lahav T, Sivam D, Volpin H, Ronen M, Tsigankov P, Green A, et al. Multiple levels of gene regulation mediate differentiation of the intracellular pathogen Leishmania. FASEB J. 2011; 25(2):515–25. doi: 10.1096/fj.10-157529 PMID: 20952481

14. Kelly S, Kramer S, Schwede A, Maini PK, Gull K, Carrington M. Genome organization is a major component of gene expression control in response to stress and during the cell division cycle in trypanosomes. Open Biol. 2012; 2(4):120033. doi: 10.1098/rsob.120033 PMID: 22724062

15. Clayton C. The regulation of trypanosome gene expression by RNA-binding proteins. PLoS Pathog. 2013; 9(11):e1003680. doi: 10.1371/journal.ppat.1003680 PMID: 24244152

16. Vasquez JJ, Hon CC, Vanselow JT, Schlosser A, Siegel TN. Comparative ribosome profiling reveals extensive translational complexity in different Trypanosoma brucei life cycle stages. Nucleic Acids Res. 2014; 42(6):3623–37. doi: 10.1093/nar/gkt1386 PMID: 24442674

17. Jensen BC, Ramasamy G, Vasconcelos EJ, Ingolia NT, Myler PJ, Parsons M. Extensive stage-regulation of translation revealed by ribosome profiling of Trypanosoma brucei. BMC Genomics. 2014; 15:911. doi: 10.1186/1471-2164-15-911 PMID: 25331479

18. Smircich P, Eastman G, Bispo S, Duhagon MA, Guerra-Slompo EP, Garat B, et al. Ribosome profiling reveals translation control as a key mechanism generating differential gene expression in Trypanosoma cruzi. BMC Genomics. 2015; 16:443. doi: 10.1186/s12864-015-1563-8 PMID: 26054634

19. Schwanhausser B, Busse D, Li N, Dittmar G, Schuchhardt J, Wolf J, et al. Global quantification of mammalian gene expression control. Nature. 2011; 473(7347):337–42. doi: 10.1038/nature10098 PMID: 21593866

20. Ouellette M, Papadopoulou B. Coordinated gene expression by post-transcriptional regulons in African trypanosomes. J Biol. 2009; 8(11):100. doi: 10.1186/jbiol203 PMID: 20017896

21. Walrad PB, Capewell P, Fenn K, Matthews KR. The post-transcriptional trans-acting regulator, TbZFP3, co-ordinates transmission-stage enriched mRNAs in Trypanosoma brucei. Nucleic Acids Res. 2012; 40(7):2869–83. doi: 10.1093/nar/gkr1106 PMID: 22140102

22. Najafabadi HS, Lu Z, MacPherson C, Mehta V, Adoue V, Pastinen T, et al. Global identification of conserved post-transcriptional regulatory programs in trypanosomatids. Nucleic Acids Res. 2013; 41 (18):8591–600. doi: 10.1093/nar/gkt647 PMID: 23877242

23. Saxena A, Lahav T, Holland N, Aggarwal G, Anupama A, Huang Y, et al. Analysis of the Leishmania donovani transcriptome reveals an ordered progression of transient and permanent changes in gene expression during differentiation. Mol Biochem Parasitol. 2007; 152(1):53–65. doi: 10.1016/j. molbiopara.2006.11.011 PMID: 17204342

24. Kolev NG, Ullu E, Tschudi C. The emerging role of RNA-binding proteins in the life cycle of Trypanosoma brucei. Cell Microbiol. 2014; 16(4):482–9. doi: 10.1111/cmi.12268 PMID: 24438230

25. Clayton CE. Networks of gene expression regulation in Trypanosoma brucei. Mol Biochem Parasitol. 2014; 195(2):96–106. doi: 10.1016/j.molbiopara.2014.06.005 PMID: 24995711

26. Keene JD. RNA regulons: coordination of post-transcriptional events. Nat Rev Genet. 2007; 8 (7):533–43. doi: 10.1038/nrg2111 PMID: 17572691

27. Gazestani VH, Lu Z, Salavati R. Deciphering RNA regulatory elements in trypanosomatids: one piece at a time or genome-wide? Trends Parasitol. 2014; 30(5):234–40. doi: 10.1016/j.pt.2014.02.008 PMID: 24642036

28. Kolev NG, Ramey-Butler K, Cross GA, Ullu E, Tschudi C. Developmental progression to infectivity in Trypanosoma brucei triggered by an RNA-binding protein. Science. 2012; 338(6112):1352–3. doi: 10. 1126/science.1229641 PMID: 23224556

29. Weston D, La Flamme AC, Van Voorhis WC. Expression of Trypanosoma cruzi surface antigen FL-160 is controlled by elements in the 3' untranslated, the 3' intergenic, and the coding regions. Mol Biochem Parasitol. 1999; 102(1):53–66. PMID: 10477176

30. Li ZH, De Gaudenzi JG, Alvarez VE, Mendiondo N, Wang H, Kissinger JC, et al. A 43-nucleotide U-rich element in 3'-untranslated region of large number of Trypanosoma cruzi transcripts is important

for mRNA abundance in intracellular amastigotes. J Biol Chem. 2012; 287(23):19058–69. doi: 10.1074/jbc.M111.338699 PMID: 22500021

31. Coughlin BC, Teixeira SM, Kirchhoff LV, Donelson JE. Amastin mRNA abundance in Trypanosoma cruzi is controlled by a 3'-untranslated region position-dependent cis-element and an untranslated region-binding protein. J Biol Chem. 2000; 275(16):12051–60. PMID: 10766837

32. Bayer-Santos E, Gentil LG, Cordero EM, Correa PR, da Silveira JF. Regulatory elements in the 3' untranslated region of the GP82 glycoprotein are responsible for its stage-specific expression in Trypanosoma cruzi metacyclic trypomastigotes. Acta Trop. 2012; 123(3):230–3. doi: 10.1016/j.actatropica.2012.03.014 PMID: 22579673

33. Alves LR, Oliveira C, Morking PA, Kessler RL, Martins ST, Romagnoli BA, et al. The mRNAs associated to a zinc finger protein from Trypanosoma cruzi shift during stress conditions. RNA Biol. 2014; 11 (7):921–33. doi: 10.4161/rna.29622 PMID: 25180711

34. De Gaudenzi JG, Carmona SJ, Aguero F, Frasch AC. Genome-wide analysis of 3'-untranslated regions supports the existence of post-transcriptional regulons controlling gene expression in trypanosomes. PeerJ. 2013; 1:e118. doi: 10.7717/peerj.118 PMID: 23904995

35. El-Sayed NM, Myler PJ, Bartholomeu DC, Nilsson D, Aggarwal G, Tran AN, et al. The genome sequence of Trypanosoma cruzi, etiologic agent of Chagas disease. Science. 2005; 309(5733):409–15. doi: 10.1126/science.1112631 PMID: 16020725

36. Trapnell C, Pachter L, Salzberg SL. TopHat: discovering splice junctions with RNA-Seq. Bioinformatics. 2009; 25(9):1105–11. doi: 10.1093/bioinformatics/btp120 PMID: 19289445

37. Grisard EC, Teixeira SM, de Almeida LG, Stoco PH, Gerber AL, Talavera-Lopez C, et al. Trypanosoma cruzi Clone Dm28c Draft Genome Sequence. Genome Announc. 2014; 2(1). doi: 10.1128/genomeA.01114-13

38. Franzen O, Ochaya S, Sherwood E, Lewis MD, Llewellyn MS, Miles MA, et al. Shotgun sequencing analysis of Trypanosoma cruzi I Sylvio X10/1 and comparison with T. cruzi VI CL Brener. PLoS Negl Trop Dis. 2011; 5(3):e984. doi: 10.1371/journal.pntd.0000984 PMID: 21408126

39. Ashburner M, Ball CA, Blake JA, Botstein D, Butler H, Cherry JM, et al. Gene ontology: tool for the unification of biology. The Gene Ontology Consortium. Nat Genet. 2000; 25(1):25–9. doi: 10.1038/75556 PMID: 10802651

40. Young MD, Wakefield MJ, Smyth GK, Oshlack A. Gene ontology analysis for RNA-seq: accounting for selection bias. Genome Biol. 2010; 11(2):R14. doi: 10.1186/gb-2010-11-2-r14 PMID: 20132535

41. Hartigan JA, Wong MA. A K-means clustering program. Journal of the Royal Statistical Society. 1979; 28:100–8.

42. Minning TA, Weatherly DB, Atwood J, 3rd, Orlando R, Tarleton RL. The steady-state transcriptome of the four major life-cycle stages of Trypanosoma cruzi. BMC Genomics. 2009; 10:370. doi: 10.1186/1471-2164-10-370 PMID: 19664227

43. Lee SC, Kim IG, Marekov LN, O'Keefe EJ, Parry DA, Steinert PM. The structure of human trichohyalin. Potential multiple roles as a functional EF-hand-like calcium-binding protein, a cornified cell envelope precursor, and an intermediate filament-associated (cross-linking) protein. J Biol Chem. 1993; 268(16):12164–76. PMID: 7685034

44. Moreno SN, Silva J, Vercesi AE, Docampo R. Cytosolic-free calcium elevation in Trypanosoma cruzi is required for cell invasion. J Exp Med. 1994; 180(4):1535–40. PMID: 7931085

45. Chuenkova MV, Furnari FB, Cavenee WK, Pereira MA. Trypanosoma cruzi trans-sialidase: a potent and specific survival factor for human Schwann cells by means of phosphatidylinositol 3-kinase/Akt signaling. Proc Natl Acad Sci U S A. 2001; 98(17):9936–41. doi: 10.1073/pnas.161298398 PMID: 11481434

46. Teixeira AA, de Vasconcelos Vde C, Colli W, Alves MJ, Giordano RJ. Trypanosoma cruzi Binds to Cytokeratin through Conserved Peptide Motifs Found in the Laminin-G-Like Domain of the gp85/Trans-sialidase Proteins. PLoS Negl Trop Dis. 2015; 9(9):e0004099. doi: 10.1371/journal.pntd.0004099 PMID: 26398185

47. Mittra B, Cortez M, Haydock A, Ramasamy G, Myler PJ, Andrews NW. Iron uptake controls the generation of Leishmania infective forms through regulation of ROS levels. J Exp Med. 2013; 210(2):401–16. doi: 10.1084/jem.20121368 PMID: 23382545

48. Koumandou VL, Natesan SK, Sergeenko T, Field MC. The trypanosome transcriptome is remodelled during differentiation but displays limited responsiveness within life stages. BMC Genomics. 2008; 9:298. doi: 10.1186/1471-2164-9-298 PMID: 18573209

49. Buscaglia CA, Campo VA, Frasch AC, Di Noia JM. Trypanosoma cruzi surface mucins: host-dependent coat diversity. Nat Rev Microbiol. 2006; 4(3):229–36. doi: 10.1038/nrmicro1351 PMID: 16489349

50. Tonelli RR, Giordano RJ, Barbu EM, Torrecilhas AC, Kobayashi GS, Langley RR, et al. Role of the gp85/trans-sialidases in Trypanosoma cruzi tissue tropism: preferential binding of a conserved peptide motif to the vasculature in vivo. PLoS Negl Trop Dis. 2010; 4(11):e864. doi: 10.1371/journal.pntd.0000864 PMID: 21072227

51. Staquicini DI, Martins RM, Macedo S, Sasso GR, Atayde VD, Juliano MA, et al. Role of GP82 in the selective binding to gastric mucin during oral infection with Trypanosoma cruzi. PLoS Negl Trop Dis. 2010; 4(3):e613. doi: 10.1371/journal.pntd.0000613 PMID: 20209152

52. Kangussu-Marcolino MM, de Paiva RM, Araujo PR, de Mendonca-Neto RP, Lemos L, Bartholomeu DC, et al. Distinct genomic organization, mRNA expression and cellular localization of members of two amastin sub-families present in Trypanosoma cruzi. BMC Microbiol. 2013; 13:10. doi: 10.1186/1471-2180-13-10 PMID: 23327097

53. Guther ML, Ferguson MA. The role of inositol acylation and inositol deacylation in GPI biosynthesis in Trypanosoma brucei. EMBO J. 1995; 14(13):3080–93. PMID: 7621823

54. Belaunzaran ML, Wilkowsky SE, Lammel EM, Gimenez G, Bott E, Barbieri MA, et al. Phospholipase A1: a novel virulence factor in Trypanosoma cruzi. Mol Biochem Parasitol. 2013; 187(2):77–86. doi: 10.1016/j.molbiopara.2012.12.004 PMID: 23275096

55. de Paulo Martins V, Okura M, Maric D, Engman DM, Vieira M, Docampo R, et al. Acylation-dependent export of Trypanosoma cruzi phosphoinositide-specific phospholipase C to the outer surface of amastigotes. J Biol Chem. 2010; 285(40):30906–17. doi: 10.1074/jbc.M110.142190 PMID: 20647312

56. Salto ML, Bertello LE, Vieira M, Docampo R, Moreno SN, de Lederkremer RM. Formation and remodeling of inositolphosphoceramide during differentiation of Trypanosoma cruzi from trypomastigote to amastigote. Eukaryot Cell. 2003; 2(4):756–68. PMID: 12912895

57. Andrews NW, Abrams CK, Slatin SL, Griffiths G. A T. cruzi-secreted protein immunologically related to the complement component C9: evidence for membrane pore-forming activity at low pH. Cell. 1990; 61(7):1277–87. PMID: 2194668

58. Marquis H, Doshi V, Portnoy DA. The broad-range phospholipase C and a metalloprotease mediate listeriolysin O-independent escape of Listeria monocytogenes from a primary vacuole in human epithelial cells. Infect Immun. 1995; 63(11):4531–4. PMID: 7591098

59. Furuya T, Kashuba C, Docampo R, Moreno SN. A novel phosphatidylinositol-phospholipase C of Trypanosoma cruzi that is lipid modified and activated during trypomastigote to amastigote differentiation. J Biol Chem. 2000; 275(9):6428–38. PMID: 10692446

60. Belaunzaran ML, Wainszelbaum MJ, Lammel EM, Gimenez G, Aloise MM, Florin-Christensen J, et al. Phospholipase A1 from Trypanosoma cruzi infective stages generates lipid messengers that activate host cell protein kinase c. Parasitology. 2007; 134(Pt 4):491–502. doi: 10.1017/S0031182006001740 PMID: 17121684

61. Cuevas IC, Rohloff P, Sanchez DO, Docampo R. Characterization of farnesylated protein tyrosine phosphatase TcPRL-1 from Trypanosoma cruzi. Eukaryot Cell. 2005; 4(9):1550–61. doi: 10.1128/EC.4.9.1550–1561.2005 PMID: 16151248

62. Gonzales-Perdomo M, Romero P, Goldenberg S. Cyclic AMP and adenylate cyclase activators stimulate Trypanosoma cruzi differentiation. Exp Parasitol. 1988; 66(2):205–12. PMID: 2840306

63. Buchanan KT, Ames JB, Asfaw SH, Wingard JN, Olson CL, Campana PT, et al. A flagellum-specific calcium sensor. J Biol Chem. 2005; 280(48):40104–11. doi: 10.1074/jbc.M505777200 PMID: 16148003

64. Gluenz E, Ginger ML, McKean PG. Flagellum assembly and function during the Leishmania life cycle. Curr Opin Microbiol. 2010; 13(4):473–9. doi: 10.1016/j.mib.2010.05.008 PMID: 20541962

65. Parsons M, Worthey EA, Ward PN, Mottram JC. Comparative analysis of the kinomes of three pathogenic trypanosomatids: Leishmania major, Trypanosoma brucei and Trypanosoma cruzi. BMC Genomics. 2005; 6:127. doi: 10.1186/1471-2164-6-127 PMID: 16164760

66. Boitz JM, Ullman B, Jardim A, Carter NS. Purine salvage in Leishmania: complex or simple by design? Trends Parasitol. 2012; 28(8):345–52. doi: 10.1016/j.pt.2012.05.005 PMID: 22726696

67. Lee SH, Stephens JL, Paul KS, Englund PT. Fatty acid synthesis by elongases in trypanosomes. Cell. 2006; 126(4):691–9. doi: 10.1016/j.cell.2006.06.045 PMID: 16923389

68. Zhang K, Hsu FF, Scott DA, Docampo R, Turk J, Beverley SM. Leishmania salvage and remodelling of host sphingolipids in amastigote survival and acidocalcisome biogenesis. Mol Microbiol. 2005; 55(5):1566–78. doi: 10.1111/j.1365-2958.2005.04493.x PMID: 15720561

69. Nishikawa Y, Quittnat F, Stedman TT, Voelker DR, Choi JY, Zahn M, et al. Host cell lipids control cholesteryl ester synthesis and storage in intracellular Toxoplasma. Cell Microbiol. 2005; 7(6):849–67. doi: 10.1111/j.1462-5822.2005.00518.x PMID: 15888087

70. Nolan SJ, Romano JD, Luechtefeld T, Coppens I. Neospora caninum Recruits Host Cell Structures to Its Parasitophorous Vacuole and Salvages Lipids from Organelles. Eukaryot Cell. 2015; 14(5):454–73. doi: 10.1128/EC.00262-14 PMID: 25750213

71. Phillips BP. The effects of various treatment procedures on the metabolism of Trypanosoma cruzi and on its ability to support growth of Endamoeba histolytica. Am J Trop Med Hyg. 1953; 2(1):47–53. PMID: 13007921

72. Warren LG. Metabolism of Schizotrypanum cruzi Chagas. I. Effect of culture age and substrate concentration on respiratory rate. J Parasitol. 1960; 46:529–39. PMID: 13783227

73. Opperdoes FR, Borst P. Localization of nine glycolytic enzymes in a microbody-like organelle in Trypanosoma brucei: the glycosome. FEBS Lett. 1977; 80(2):360–4. PMID: 142663

74. Leroux AE, Maugeri DA, Cazzulo JJ, Nowicki C. Functional characterization of NADP-dependent isocitrate dehydrogenase isozymes from Trypanosoma cruzi. Mol Biochem Parasitol. 2011; 177(1):61–4. doi: 10.1016/j.molbiopara.2011.01.010 PMID: 21291916

75. Rogerson GW, Gutteridge WE. Oxidative metabolism in mammalian and culture forms of Trypanosoma cruzi. Int J Biochem. 1979; 10(12):1019–23. PMID: 229013

76. Stoppani AO, Docampo R, de Boiso JF, Frasch AC. Effect of inhibitors of electron transport and oxidative phosphorylation on Trypanosoma cruzi respiration and growth. Mol Biochem Parasitol. 1980; 2 (1):3–21. PMID: 7007881

77. Adroher FJ, Osuna A, Lupianez JA. Differential energetic metabolism during Trypanosoma cruzi differentiation. I. Citrate synthase, NADP-isocitrate dehydrogenase, and succinate dehydrogenase. Arch Biochem Biophys. 1988; 267(1):252–61. PMID: 3058038

78. Adroher FJ, Osuna A, Lupianez JA. Differential energetic metabolism during Trypanosoma cruzi differentiation. II. Hexokinase, phosphofructokinase and pyruvate kinase. Mol Cell Biochem. 1990; 94 (1):71–82. PMID: 2143268

79. Silber AM, Tonelli RR, Lopes CG, Cunha-e-Silva N, Torrecilhas AC, Schumacher RI, et al. Glucose uptake in the mammalian stages of Trypanosoma cruzi. Mol Biochem Parasitol. 2009; 168(1):102–8. doi: 10.1016/j.molbiopara.2009.07.006 PMID: 19631694

80. Rogerson GW, Gutteridge WE. Catabolic metabolism in Trypanosoma cruzi. Int J Parasitol. 1980; 10 (2):131–5. PMID: 6989775

81. Brand MD, Nicholls DG. Assessing mitochondrial dysfunction in cells. Biochem J. 2011; 435(2):297–312. doi: 10.1042/BJ20110162 PMID: 21726199

82. Sriskanthadevan S, Jeyaraju DV, Chung TE, Prabha S, Xu W, Skrtic M, et al. AML cells have low spare reserve capacity in their respiratory chain that renders them susceptible to oxidative metabolic stress. Blood. 2015; 125(13):2120–30. doi: 10.1182/blood-2014-08-594408 PMID: 25631767

83. Villani G, Attardi G. In vivo control of respiration by cytochrome c oxidase in human cells. Free Radic Biol Med. 2000; 29(3–4):202–10. PMID: 11035248

84. Horvath A, Horakova E, Dunajcikova P, Verner Z, Pravdova E, Slapetova I, et al. Downregulation of the nuclear-encoded subunits of the complexes III and IV disrupts their respective complexes but not complex I in procyclic Trypanosoma brucei. Mol Microbiol. 2005; 58(1):116–30. doi: 10.1111/j.1365-2958.2005.04813.x PMID: 16164553

85. Dey R, Meneses C, Salotra P, Kamhawi S, Nakhasi HL, Duncan R. Characterization of a Leishmania stage-specific mitochondrial membrane protein that enhances the activity of cytochrome c oxidase and its role in virulence. Mol Microbiol. 2010; 77(2):399–414. doi: 10.1111/j.1365-2958.2010.07214.x PMID: 20497506

86. Cardenas D, Carter PM, Nation CS, Pizarro JC, Guidry J, Aiyar A, et al. LACK, a RACK1 ortholog, facilitates cytochrome c oxidase subunit expression to promote Leishmania major fitness. Mol Microbiol. 2015; 96(1):95–109. doi: 10.1111/mmi.12924 PMID: 25582232

87. Atwood JA 3rd, Weatherly DB, Minning TA, Bundy B, Cavola C, Opperdoes FR, et al. The Trypanosoma cruzi proteome. Science. 2005; 309(5733):473–6. doi: 10.1126/science.1110289 PMID: 16020736

88. Urbina JA, Azavache V. Regulation of energy metabolism in Trypanosoma (Schizotrypanum) cruzi epimastigotes. II. NAD+-dependent glutamate dehydrogenase. Mol Biochem Parasitol. 1984; 11:241–55. PMID: 6379448

89. Juan SM, Segura EL, Cazzulo JJ. Purification and some properties of the NADP-linked glutamate dehydrogenase from Trypanosoma cruzi. Int J Biochem. 1978; 9(6):395–400. PMID: 27404

90. Walter RD, Ebert F. Evidence for NADH- and NADPH-linked glutamate dehydrogenases in Trypanosoma cruzi epimastigotes. J Protozool. 1979; 26(4):653–6. PMID: 44525

91. Winter RW, Kelly JX, Smilkstein MJ, Dodean R, Hinrichs D, Riscoe MK. Antimalarial quinolones: synthesis, potency, and mechanistic studies. Exp Parasitol. 2008; 118(4):487–97. doi: 10.1016/j. exppara.2007.10.016 PMID: 18082162

92. Winter R, Kelly JX, Smilkstein MJ, Hinrichs D, Koop DR, Riscoe MK. Optimization of endochin-like quinolones for antimalarial activity. Exp Parasitol. 2011; 127(2):545–51. doi: 10.1016/j.exppara.2010. 10.016 PMID: 21040724

93. Doggett JS, Nilsen A, Forquer I, Wegmann KW, Jones-Brando L, Yolken RH, et al. Endochin-like quinolones are highly efficacious against acute and latent experimental toxoplasmosis. Proc Natl Acad Sci U S A. 2012; 109(39):15936–41. doi: 10.1073/pnas.1208069109 PMID: 23019377

94. Khare S, Roach SL, Barnes SW, Hoepfner D, Walker JR, Chatterjee AK, et al. Utilizing Chemical Genomics to Identify Cytochrome b as a Novel Drug Target for Chagas Disease. PLoS Pathog. 2015; 11(7):e1005058. doi: 10.1371/journal.ppat.1005058 PMID: 26186534

95. Brown RC, Evans DA, Vickerman K. Changes in oxidative metabolism and ultrastructure accompanying differentiation of the mitochondrion in Trypanosoma brucei. Int J Parasitol. 1973; 3(5):691–704. PMID: 4354962

96. Overath P, Czichos J, Haas C. The effect of citrate/cis-aconitate on oxidative metabolism during transformation of Trypanosoma brucei. Eur J Biochem. 1986; 160(1):175–82. PMID: 3769918

97. Priest JW, Hajduk SL. Developmental regulation of Trypanosoma brucei cytochrome c reductase during bloodstream to procyclic differentiation. Mol Biochem Parasitol. 1994; 65(2):291–304. PMID: 7969270

98. Barnard JP, Pedersen PL. Alteration of pyruvate metabolism in African trypanosomes during differentiation from bloodstream into insect forms. Arch Biochem Biophys. 1994; 313(1):77–82. doi: 10.1006/ abbi.1994.1361 PMID: 8053690

99. Ghosh AK, Sardar AH, Mandal A, Saini S, Abhishek K, Kumar A, et al. Metabolic reconfiguration of the central glucose metabolism: a crucial strategy of Leishmania donovani for its survival during oxidative stress. FASEB J. 2015; 29(5):2081–98. doi: 10.1096/fj.14-258624 PMID: 25690656

100. Vaena de Avalos S, Blader IJ, Fisher M, Boothroyd JC, Burleigh BA. Immediate/early response to Trypanosoma cruzi infection involves minimal modulation of host cell transcription. J Biol Chem. 2002; 277(1):639–44. doi: 10.1074/jbc.M109037200 PMID: 11668183

101. Mukherjee S, Belbin TJ, Spray DC, Iacobas DA, Weiss LM, Kitsis RN, et al. Microarray analysis of changes in gene expression in a murine model of chronic chagasic cardiomyopathy. Parasitol Res. 2003; 91(3):187–96. doi: 10.1007/s00436-003-0937-z PMID: 12910413

102. Moore-Lai D, Rowland E. Microarray data demonstrate that Trypanosoma cruzi downregulates the expression of apoptotic genes in BALB/c fibroblasts. J Parasitol. 2004; 90(4):893–5. doi: 10.1645/GE-146R PMID: 15357096

103. Imai K, Mimori T, Kawai M, Koga H. Microarray analysis of host gene-expression during intracellular nests formation of Trypanosoma cruzi amastigotes. Microbiol Immunol. 2005; 49(7):623–31. PMID: 16034205

104. Hashimoto M, Nakajima-Shimada J, Ishidoh K, Aoki T. Gene expression profiles in response to Fas stimulation in Trypanosoma cruzi-infected host cells. Int J Parasitol. 2005; 35(14):1587–94. doi: 10. 1016/j.ijpara.2005.08.004 PMID: 16185694

105. Shigihara T, Hashimoto M, Shindo N, Aoki T. Transcriptome profile of Trypanosoma cruzi-infected cells: simultaneous up- and down-regulation of proliferation inhibitors and promoters. Parasitol Res. 2008; 102(4):715–22. doi: 10.1007/s00436-007-0819-x PMID: 18058129

106. Chessler AD, Unnikrishnan M, Bei AK, Daily JP, Burleigh BA. Trypanosoma cruzi triggers an early type I IFN response in vivo at the site of intradermal infection. J Immunol. 2009; 182(4):2288–96. doi: 10.4049/jimmunol.0800621 PMID: 19201883

107. Costales JA, Daily JP, Burleigh BA. Cytokine-dependent and-independent gene expression changes and cell cycle block revealed in Trypanosoma cruzi-infected host cells by comparative mRNA profiling. BMC Genomics. 2009; 10:252. doi: 10.1186/1471-2164-10-252 PMID: 19480704

108. Adesse D, Iacobas DA, Iacobas S, Garzoni LR, Meirelles Mde N, Tanowitz HB, et al. Transcriptomic signatures of alterations in a myoblast cell line infected with four distinct strains of Trypanosoma cruzi. Am J Trop Med Hyg. 2010; 82(5):846–54. doi: 10.4269/ajtmh.2010.09–0399 PMID: 20439965

109. Nde PN, Johnson CA, Pratap S, Cardenas TC, Kleshchenko YY, Furtak VA, et al. Gene network analysis during early infection of human coronary artery smooth muscle cells by Trypanosoma cruzi and Its gp83 ligand. Chem Biodivers. 2010; 7(5):1051–64. doi: 10.1002/cbdv.200900320 PMID: 20491065

110. Tanowitz HB, Mukhopadhyay A, Ashton AW, Lisanti MP, Machado FS, Weiss LM, et al. Microarray analysis of the mammalian thromboxane receptor-Trypanosoma cruzi interaction. Cell Cycle. 2011; 10(7):1132–43. PMID: 21364319

111. Bafica A, Santiago HC, Goldszmid R, Ropert C, Gazzinelli RT, Sher A. Cutting edge: TLR9 and TLR2 signaling together account for MyD88-dependent control of parasitemia in Trypanosoma cruzi infection. J Immunol. 2006; 177(6):3515–9. PMID: 16951309

112. Chessler AD, Ferreira LR, Chang TH, Fitzgerald KA, Burleigh BA. A novel IFN regulatory factor 3-dependent pathway activated by trypanosomes triggers IFN-beta in macrophages and fibroblasts. J Immunol. 2008; 181(11):7917–24. PMID: 19017982

113. Silva GK, Gutierrez FR, Guedes PM, Horta CV, Cunha LD, Mineo TW, et al. Cutting edge: nucleotide-binding oligomerization domain 1-dependent responses account for murine resistance against Trypanosoma cruzi infection. J Immunol. 2010; 184(3):1148–52. doi: 10.4049/jimmunol.0902254 PMID: 20042586

114. Caetano BC, Carmo BB, Melo MB, Cerny A, dos Santos SL, Bartholomeu DC, et al. Requirement of UNC93B1 reveals a critical role for TLR7 in host resistance to primary infection with Trypanosoma cruzi. J Immunol. 2011; 187(4):1903–11. doi: 10.4049/jimmunol.1003911 PMID: 21753151

115. Silva GK, Costa RS, Silveira TN, Caetano BC, Horta CV, Gutierrez FR, et al. Apoptosis-associated speck-like protein containing a caspase recruitment domain inflammasomes mediate IL-1beta response and host resistance to Trypanosoma cruzi infection. J Immunol. 2013; 191(6):3373–83. doi: 10.4049/jimmunol.1203293 PMID: 23966627

116. Goncalves VM, Matteucci KC, Buzzo CL, Miollo BH, Ferrante D, Torrecilhas AC, et al. NLRP3 controls Trypanosoma cruzi infection through a caspase-1-dependent IL-1R-independent NO production. PLoS Negl Trop Dis. 2013; 7(10):e2469. doi: 10.1371/journal.pntd.0002469 PMID: 24098823

117. Chessler AD, Caradonna KL, Da'dara A, Burleigh BA. Type I interferons increase host susceptibility to Trypanosoma cruzi infection. Infect Immun. 2011; 79(5):2112–9. doi: 10.1128/IAI.01176-10 PMID: 21402764

118. Stifter SA, Feng CG. Interfering with immunity: detrimental role of type I IFNs during infection. J Immunol. 2015; 194(6):2455–65. doi: 10.4049/jimmunol.1402794 PMID: 25747907

119. Caradonna KL, Engel JC, Jacobi D, Lee CH, Burleigh BA. Host metabolism regulates intracellular growth of Trypanosoma cruzi. Cell Host Microbe. 2013; 13(1):108–17. doi: 10.1016/j.chom.2012.11.011 PMID: 23332160

120. Horton JD, Goldstein JL, Brown MS. SREBPs: activators of the complete program of cholesterol and fatty acid synthesis in the liver. J Clin Invest. 2002; 109(9):1125–31. doi: 10.1172/JCI15593 PMID: 11994399

121. Galea AM, Brown AJ. Special relationship between sterols and oxygen: were sterols an adaptation to aerobic life? Free Radic Biol Med. 2009; 47(6):880–9. doi: 10.1016/j.freeradbiomed.2009.06.027 PMID: 19559787

122. Cavazzuti A, Paglietti G, Hunter WN, Gamarro F, Piras S, Loriga M, et al. Discovery of potent pteridine reductase inhibitors to guide antiparasite drug development. Proc Natl Acad Sci U S A. 2008; 105 (5):1448–53. doi: 10.1073/pnas.0704384105 PMID: 18245389

123. Martin JL, Yates PA, Soysa R, Alfaro JF, Yang F, Burnum-Johnson KE, et al. Metabolic reprogramming during purine stress in the protozoan pathogen Leishmania donovani. PLoS Pathog. 2014; 10 (2):e1003938. doi: 10.1371/journal.ppat.1003938 PMID: 24586154

124. Araujo PR, Teixeira SM. Regulatory elements involved in the post-transcriptional control of stage-specific gene expression in Trypanosoma cruzi: a review. Mem Inst Oswaldo Cruz. 2011; 106(3):257–66. PMID: 21655811

125. Kramer S. Developmental regulation of gene expression in the absence of transcriptional control: the case of kinetoplastids. Mol Biochem Parasitol. 2012; 181(2):61–72. doi: 10.1016/j.molbiopara.2011.10.002 PMID: 22019385

126. Perez-Morales D, Lanz-Mendoza H, Hurtado G, Martinez-Espinosa R, Espinoza B. Proteomic analysis of Trypanosoma cruzi epimastigotes subjected to heat shock. J Biomed Biotechnol. 2012; 2012:902803. doi: 10.1155/2012/902803 PMID: 22287837

127. Bayer-Santos E, Aguilar-Bonavides C, Rodrigues SP, Cordero EM, Marques AF, Varela-Ramirez A, et al. Proteomic analysis of Trypanosoma cruzi secretome: characterization of two populations of extracellular vesicles and soluble proteins. J Proteome Res. 2013; 12(2):883–97. doi: 10.1021/pr300947g PMID: 23214914

128. Queiroz RM, Charneau S, Motta FN, Santana JM, Roepstorff P, Ricart CA. Comprehensive proteomic analysis of Trypanosoma cruzi epimastigote cell surface proteins by two complementary methods. J Proteome Res. 2013; 12(7):3255–63. doi: 10.1021/pr400110h PMID: 23682730

129. Sadok Menna-Barreto RF, Belloze KT, Perales J, Silva-Jr FP. Proteomic and bioinformatic analysis of Trypanosoma cruzi chemotherapy and potential drug targets: new pieces for an old puzzle. Curr Drug Targets. 2014; 15(3):255–71. PMID: 24041335

130. Machin A, Telleria J, Brizard JP, Demettre E, Seveno M, Ayala FJ, et al. Trypanosoma cruzi: gene expression surveyed by proteomic analysis reveals interaction between different genotypes in mixed in vitro cultures. PLoS One. 2014; 9(4):e95442. doi: 10.1371/journal.pone.0095442 PMID: 24748035

131. Vieira HG, Grynberg P, Bitar M, Pires Sda F, Hilario HO, Macedo AM, et al. Proteomic analysis of Trypanosoma cruzi response to ionizing radiation stress. PLoS One. 2014; 9(5):e97526. doi: 10.1371/journal.pone.0097526 PMID: 24842666

132. Queiroz RM, Charneau S, Mandacaru SC, Schwammle V, Lima BD, Roepstorff P, et al. Quantitative proteomic and phosphoproteomic analysis of Trypanosoma cruzi amastigogenesis. Mol Cell Proteomics. 2014; 13(12):3457–72. doi: 10.1074/mcp.M114.040329 PMID: 25225356

133. Brunoro GV, Caminha MA, Ferreira AT, Leprevost Fda V, Carvalho PC, Perales J, et al. Reevaluating the Trypanosoma cruzi proteomic map: The shotgun description of bloodstream trypomastigotes. J Proteomics. 2015; 115:58–65. doi: 10.1016/j.jprot.2014.12.003 PMID: 25534883

134. P S L.H., Nussenzweig V. Sobre uma cepa de Trypanosoma cruzi altamente virulenta para o camundongo branco. Folia Clin Biol. 1953; 20:191–203.

135. Anders S, McCarthy DJ, Chen Y, Okoniewski M, Smyth GK, Huber W, et al. Count-based differential expression analysis of RNA sequencing data using R and Bioconductor. Nat Protoc. 2013; 8 (9):1765–86. doi: 10.1038/nprot.2013.099 PMID: 23975260

136. Smyth GK. Limma: linear models for microarray data. VC R. Gentleman, Dudoit S., Irizarry R., Huber W., editor. New York: Springer; 2005. 397–420 p.

137. Smyth GK. Linear models and empirical bayes methods for assessing differential expression in microarray experiments. Stat Appl Genet Mol Biol. 2004; 3(1).

138. Storey J. A direct approach to false discovery rates. Journal of the Royal Statistical Society. 2002; 64 (479–498).

139. Pearson WR. Flexible sequence similarity searching with the FASTA3 program package. Methods Mol Biol. 2000; 132:185–219. PMID: 10547837

140. Tan P-N, Steinbach M, Kumar V. Introduction to Data Mining. First Edition ed: Pearson; 2005. 769 p.

141. Benjamini Y, Hochberg Y. Controlling the False Discovery Rate: A Practical and Powerful Approach to Multiple Testing. Journal of the Royal Statistical Society. 1995; 57(1):289–300.

142. Buckner FS, Wilson AJ, Van Voorhis WC. Detection of live Trypanosoma cruzi in tissues of infected mice by using histochemical stain for beta-galactosidase. Infect Immun. 1999; 67(1):403–9. PMID: 9864242